IMPROVEMENT OF THE ENVIRONMENTAL AND ECONOMIC CHARACTERISTICS OF COOLING TOWERS

PART II of II: THE PERIODIC COOLING TOWER - FLOW VISUALIZATION, SURFACE ROUGHENING, AND FULL SCALE MODEL

by

Pou Cheong Hon
Je-Chin Han
Paul F. Pilger
Leon R. Glicksman
Warren M. Rohsenow

Energy Laboratory
in association with
Heat Transfer Laboratory
Department of Mechanical Engineering
MASSACHUSETTS INSTITUTE OF TECHNOLOGY

Sponsored by:
Empire State Electric Energy Research Corporation
New York

Energy Lab Report No. MIT-EL 74-008
Heat Transfer Lab Report No. 80047-85

June 30, 1974

ABSTRACT

The concept of periodic towers is to have sheet metal discs partially submerged in hot, power plant condenser effluent. As the discs rotate, local sections of the discs alternately absorb heat from the effluent and discharge heat to the air. The means of heat transfer on the air side can be either evaporative and/or convective, depending upon the amount of effluent carried into the air side on the surface of the plates. An oil layer, floated on the water's surface, has been shown to be effective in eliminating water carry-over to the air side.

The advantages of the periodic tower lie in the low cost of the discs and the ability to operate dry. A periodic tower is significantly less expensive than a conventional dry tower fabricated with finned tubes. Further, with the capacity of being operated wet, the high capacity losses incurred during warm months by finned tube towers can be eliminated.

The effort to evaluate periodic cooling towers has been a three-pronged thrust:

1) A full scale model of a periodic heat exchanger was designed and is being built to optimize the overall performance and determine the economic competitiveness of this new form of heat exchanger. In the periodic exchanger cooling air is forced over the top portion of a long horizontal row of circular discs slowly rotating in a hot water bath. This large model, over twenty-five feet long and ten feet high with a two and one half by one foot test section, will provide actual test data to verify previous performance optimization calculations and allow for research and development to continue on many design details for this new concept.

2) Disc Ribbing - Roughened Surfaces

An existing computer design routine for optimizing periodic cooling towers has been modified by increasing the number of variables from 5 to 8. This was done to account for the effects of roughened surfaces on heat exchanger performance. The modified optimum computer design program yields a periodic tower configuration having the lowest incremental cost for power operation, but it is impractical because the optimized rib heights are smaller than the oil film clinging to the discs. Taking into account the effect of

the coating oil thickness on the surfaces, sensitivity studies on the influences of the roughened surfaces on the incremental cost have been made. A specific 5 ft. diameter roughened surface heat exchanger yields a 15 to 20% savings of capital and incremental cost over a smooth heat exchanger of the same diameter. This economically warrants the use of roughened rather than smooth surfaces for periodic heat exchangers.

3) Flow visualization tests indicate that the mixing of water in the periodic exchanger trough is strongly dependent upon both the water's inlet and outlet points, and the rotational direction of the plates. Various mixing currents in the trough for different geometries have been observed by use of dye injection. Silicone oils, because of their lower vapor pressure and subsequent low rate of evaporation, appear to be superior to petroleum based oils.

ACKNOWLEDGEMENTS

The Empire State Electric Energy Research Corporation (ESEERCO) sponsored this study. Their support is gratefully acknowledged.

Special thanks are due to Leonard Geller, Paul Torpey, Art Sugden, Howard Philipp, and other members of the ESEERCO technical committee. Their active interest and suggestions were a great benefit to the program.

TABLE OF CONTENTS

LIST OF FIGURES

LIST OF TABLES

NOMENCLATURE

A	=	projected area of a body on a plane normal to the flow
CAPIT	=	total capital cost of adding heat exchanger to power plant
C_d	=	drag coefficient
D	=	plate spacing
DIA	=	plate diameter
DEQ	=	hydraulic diameter
E	=	rib height
Eff	=	heat exchanger effectiveness
F_1	=	frontal area of the screen cross section
F_2	=	the remainder resulting when the projected area of the screen wires is subtracted from the frontal area of the screen cross section
F_3	=	the projected area of the screen wires
f	=	friction factor
$\bar{f}$	=	ratio of projected areas of screen wires
G	=	mass flow rate
g_o	=	constant: 32.2 lbm ft/eff sec^2
h	=	heat transfer coefficient
INCREM	=	incremental generating cost resulting from use of cooling tower
K	=	the pressure drop through one screen in units of dynamic press.
K_1	=	loss coefficient
N	=	number of plates
n	=	number of screens
p	=	distance between ribs
P	=	true static pressure
Pr	=	Prandtl number
q	=	dynamic pressure of a fluid for a given Reynolds number
Q_{plate}	=	heat rejected per plate
R	=	disc radius
r	=	radial distance
r_o	=	distance disc axis above oil surface
Re	=	Reynolds number
T	=	turbulence factor
U	=	root mean square of the three principal Cartesian coordinate directions

V = fluid velocity

W = water flow rate in ducting

X = distance in inches measured along the centerline of the contraction cone

Y = the vertical distance in feet measured from the centerline of the contraction cone

Z = loss factor

GREEK SYMBOLS

ρ = fluid density

σ = surface tension

ζ = screen resistance coefficient

δ = thickness

ξ = the distance in feet measured along the centerline of the contraction cone

μ = viscosity

ω = angular velocity

ΔV = velocity perturbation in the vicinity of a screen

ΔP = difference of static pressures measured in inches of water

Δp = pressure drop

SUBSCRIPTS

a = air

av = average

c = critical

e = effective

j = jet

p = pipe

tot = total

w = water

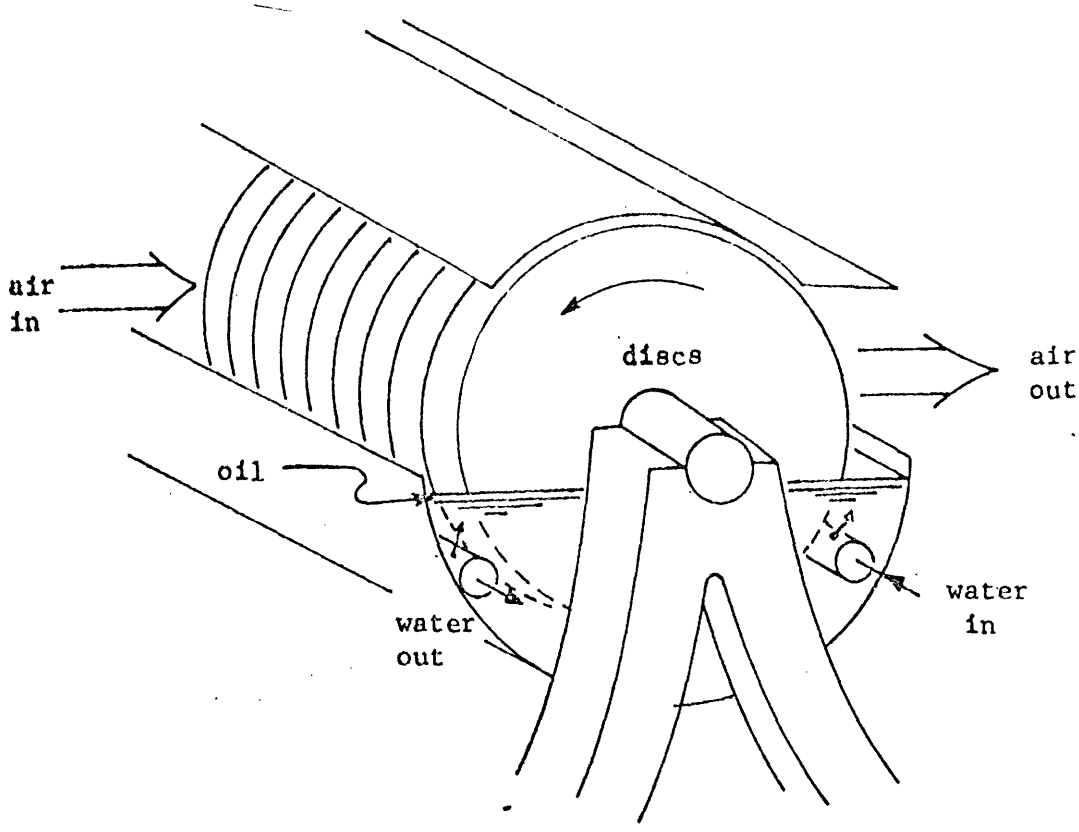

Conceptual design of periodic heat exchanger

Figure 1

I. Introduction

The summary for the year's research on the improvement of the environmental and economic characteristics of cooling towers is encompassed in two separately bound volumes. This report constitutes Part II. Part I covers heat rejection from horizontal tubes to shallow fluidized beds.

Periodic towers, along with wet and dry towers provide an alternative to once through cooling for power plant heat rejection. The adaptation of towers reduces the ecological impact of power plant waste thermal energy to the environs.

The concept of the periodic tower is to add an intermediary and interactive material between the heat source and sink. The material periodically passes from source to sink and back to source, absorbing heat from the source, and discharging heat to the sink. In power plant applications, where water (source) and air (sink) are the working fluids, heat transfer on the air side can be accomplished by either evaporative (mass transfer) or convective means, depending upon whether the intermediary surface is wet or dry. Operated dry, the tower is less dependent upon local water supplies. Operated wet, the large generating capacity losses conventional dry towers experience during hot weather can be eliminated.

Conceptually, periodic towers consist of an assembly of sheet steel discs with a common, single, axis. Each disc is parallel to its neighbor, and separated from it by a fraction of an inch. The rotating assembly is partially submerged in a trough of hot water. During rotation, local sections of each disc are periodically heated by the hot water and cooled by air drawn through the spacings between the discs.

The ground work on periodic towers was reported in part II of last year's annual report. It was found that by floating a layer of oil on the water's surface, water is no longer carried on the discs to the air side of the heat exchanger. Thus the oil layer, by eliminating all air-water interfaces, virtually eliminated evaporative water losses. The oil film has a secondary beneficial use. By constantly bathing the discs in oil, disc corrosion is eliminated, and inexpensive low carbon steel can be used for the discs. The conceptual design of the periodic heat exchanger is illustrated in Figure 1.

The periodic tower with an oil film combines the best conceptual features of the wet and the dry tower; a low cost heat exchanger surface (low carbon steel) and a low or negligible rate of water consumption.

Last year's report indicated that the periodic tower, besides having negligible evaporation like a conventional dry tower, was significantly less expensive than finned surfaces. This past year's work investigated refinements and more specific areas to further test and improve the performance of the periodic exchanger.

Investigations were centered in three main efforts:

(1) Fluid mixing. A model dimensionally similar to a full sized periodic exchanger was tested to determine the mixing of the water due to the rotation of the plates. The effort is to achieve as high a disc temperature as possible just prior to leaving the water trough. Implicit in this is properly locating the trough's water source and drain so as to prevent the entering water to pass directly to the drain.

(2) Disc ribbing. The greatest resistance to heat transfer lies in the air side of the disc assembly. Adding ribs or roughness to the disc surface 'trips' the boundary layer and effectively increases the air side heat transfer coefficient. The effort in this area has been both experimental and analytic.

(3) Full scale section of the periodic tower. A one foot thick assembly of 5' diameter discs and the associated air and water delivery system are being constructed in order to test the performance of a full sized section of the periodic concept.

These three areas of investigation are more completely discussed in the following sections.

II. Fluid Mixing - Flow Visualization

II.1 Small Model of Rotary Heat Exchanger

A small model of the rotary heat exchanger was constructed. The model was scaled to 1/3 of the full-scale size suggested by Robertson[1], The model and its sub-system are described in the following three sections.

II.1.1 Rotary Plates System

The circular plates of the model rotary heat exchanger are made of 0.040 inch thick galvanized steel. Fourteen 20 inch diameter plates, spaced 0.33 inch apart, were mounted on a 1 1/8 inch diameter shaft. The circular plates were properly separated by spacers at 5 locations as shown in Fig. 2. The 4 spacers along the circumference of the plate were made of a 0.5 inch diameter copper tube. The center spacer was sliced out of a 3 inch diameter aluminum rod, and a hole of the shaft diameter was drilled through the center of each aluminum spacer. The thickness of the spacers was machined with a tolerance of 5 mils. The spacers were held in proper positions by passing a 1/4 inch threaded rod through the plates and spacers with nuts tightened on the ends of the threaded rod protruding from the two side plates.

The shaft on which the circular plates were mounted was supported by 2 bearings. One end of the shaft is coupled to a pulley. The shaft was driven by a driving belt which was connected to a variable-speed motor. A sketch of the rotary plates system is given in Figure 3.

II.1.2 Circulating Water System

The circulating water system of the model rotary heat exchanger is best explained with the help of the fluid circuit diagram of Figure 4.

A semi-circular trough made of plexiglas was used to contain the circulating water to be cooled by the rotating plates. The water coming out from the trough was heated up as it passed the immersion heater. The pump provided a circulation of the water through the system and a constant supply of hot water into the trough. The power dissipated by the immersion heater was controlled by a variac. An ammeter and a voltmeter were connnected to the variac to measure this amount of heat dissipated to the circulating water. A rotameter was placed in series to the fluid circuit to measure the flowrate of the water.

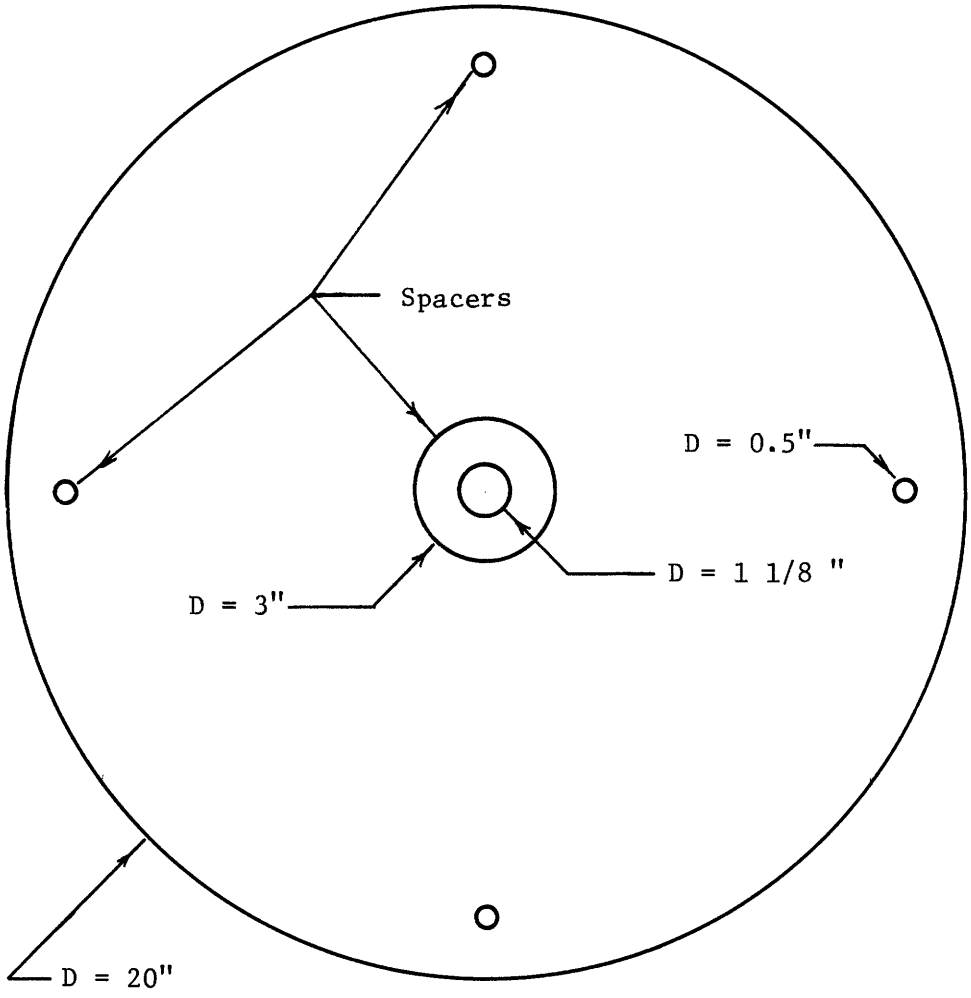

Circular Plate with Spacers

Figure 2

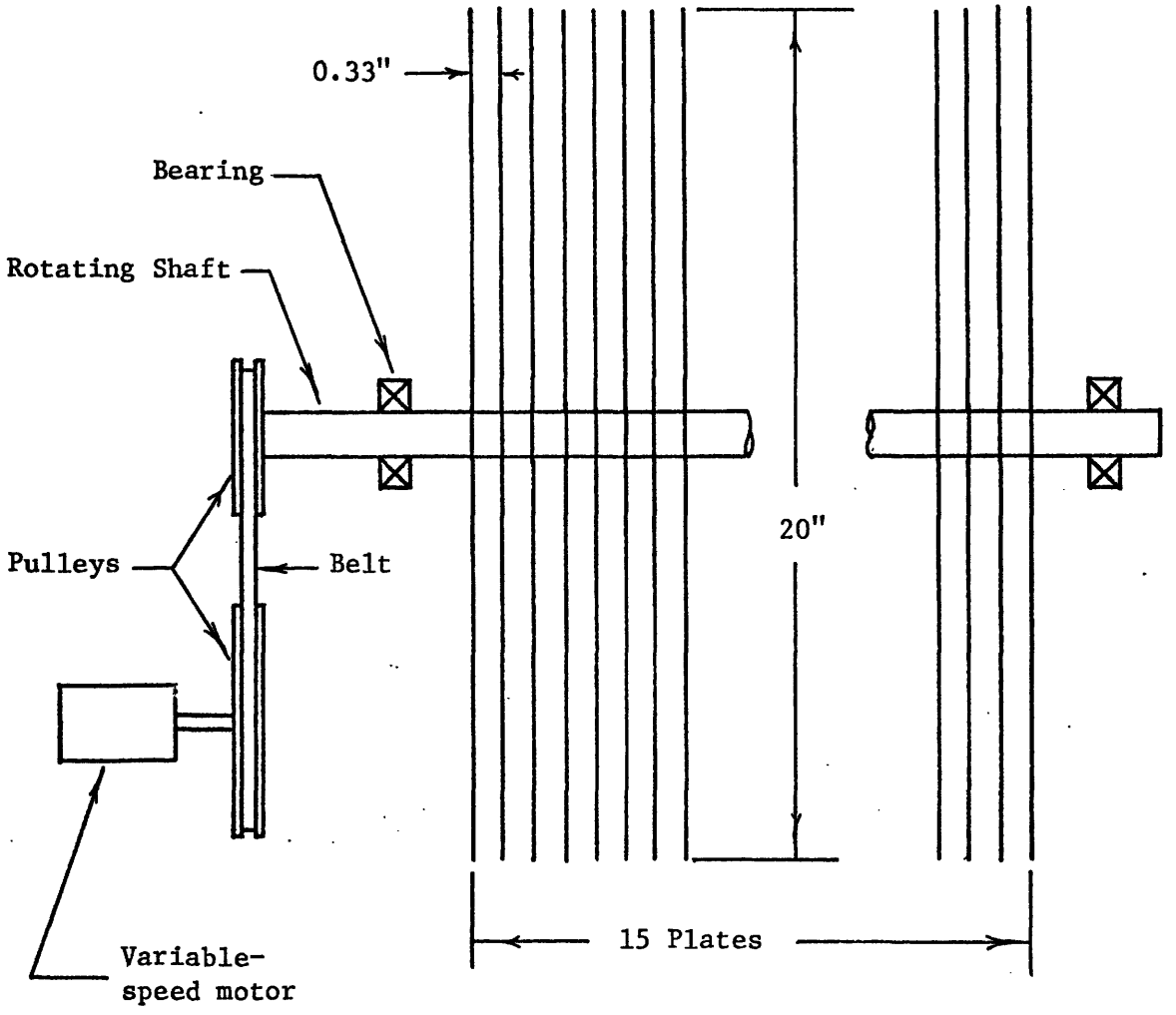

Rotary Heat Exchanger Model Schema

Figure 3

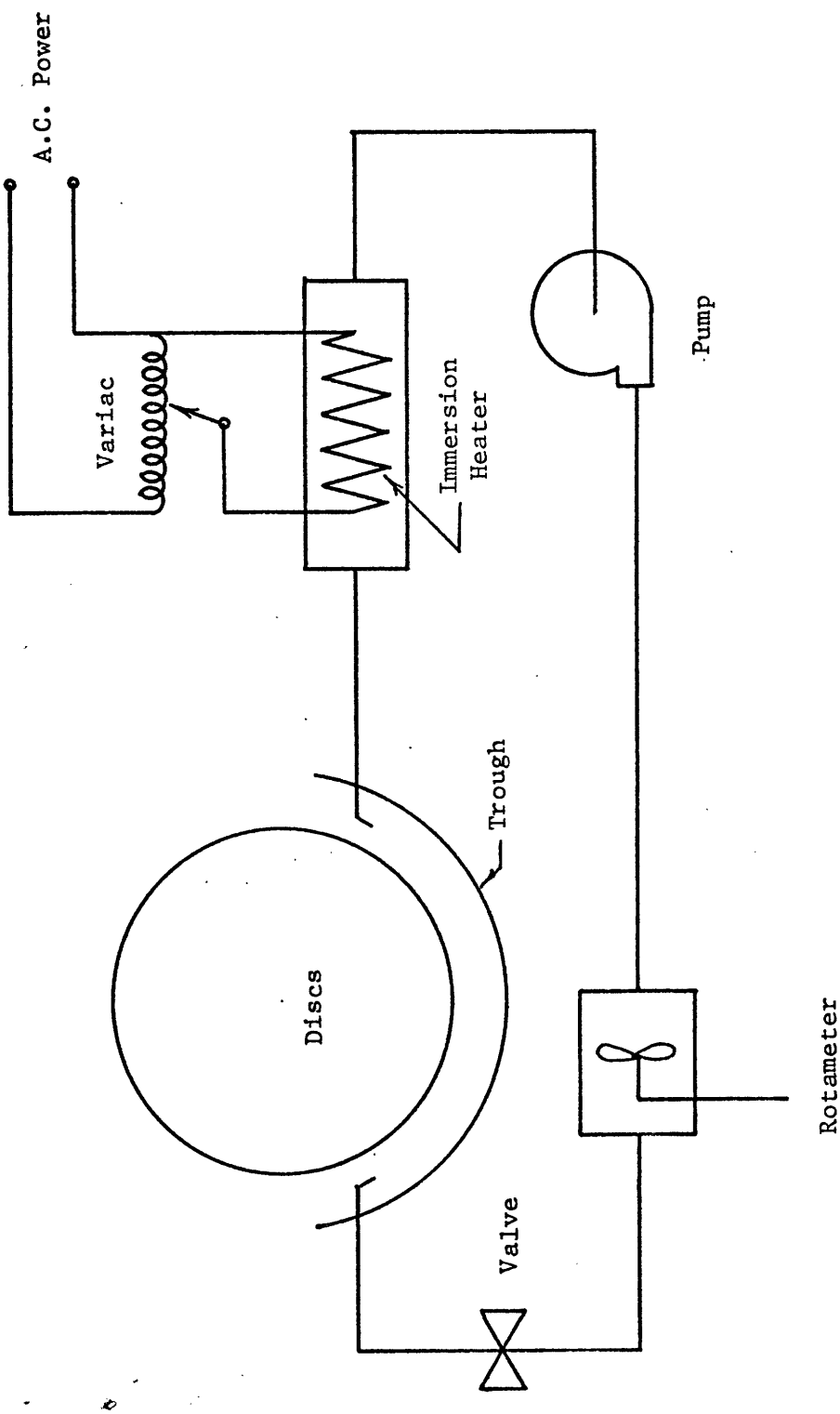

Fluid Circuit Schema

Figure 4

II.1.3 Air Flow System

The upper portion of the rotating plates of the model rotary heat exchanger was covered with an air duct. An exhaust fan was installed at the outlet of the air duct to provide air flow through the rotating plates. Since the resistance to air flow through the top of the circular plates is much smaller than that through the center of the plates, the majority of air would pass through the top of the plates if a simple rectangular air duct with a uniform air supply was used. This reduces the heat transfer effectiveness of the rotary heat exchanger as there is less area for heat transfer near the top of the plates. To prevent this, the air duct was designed as shown in Figure 5 to decrease the air flow through the top of the plates. With reduced air flow through the top, more air would pass through the center portion of the plates where there is more area for heat transfer. The inlet of the air duct was extended to a length of 40 inches to ensure a uniform air supply.

The velocity of the air flowing through the rotating plates was measured with a pitot tube located down stream of the rotating plates. The pitot tube can move vertically along the air duct's center-line as well as horizontally traverse the air duct at the mid-height of the air duct. By measuring the air velocity at different locations inside the air duct, the uniformity of the air flow can be determined.

II.2 Flow Visualization Tests

Flow visualization tests were performed to determine the flow pattern of the water in the trough. A knowledge of the flow pattern is important in that the flow pattern of the water determines the temperature profile of the rotating plates which in turn determines the heat transfer. Care must be taken to ensure the hot water entering the trough does not get pumped out directly through the outlet. To achieve a better heat transfer, it is preferred to have the hot water entering the trough have as long a contact time with the rotating plates as possible and to have the plates attain the temperature of the in-coming circulating water as the plates rotate out of the water.

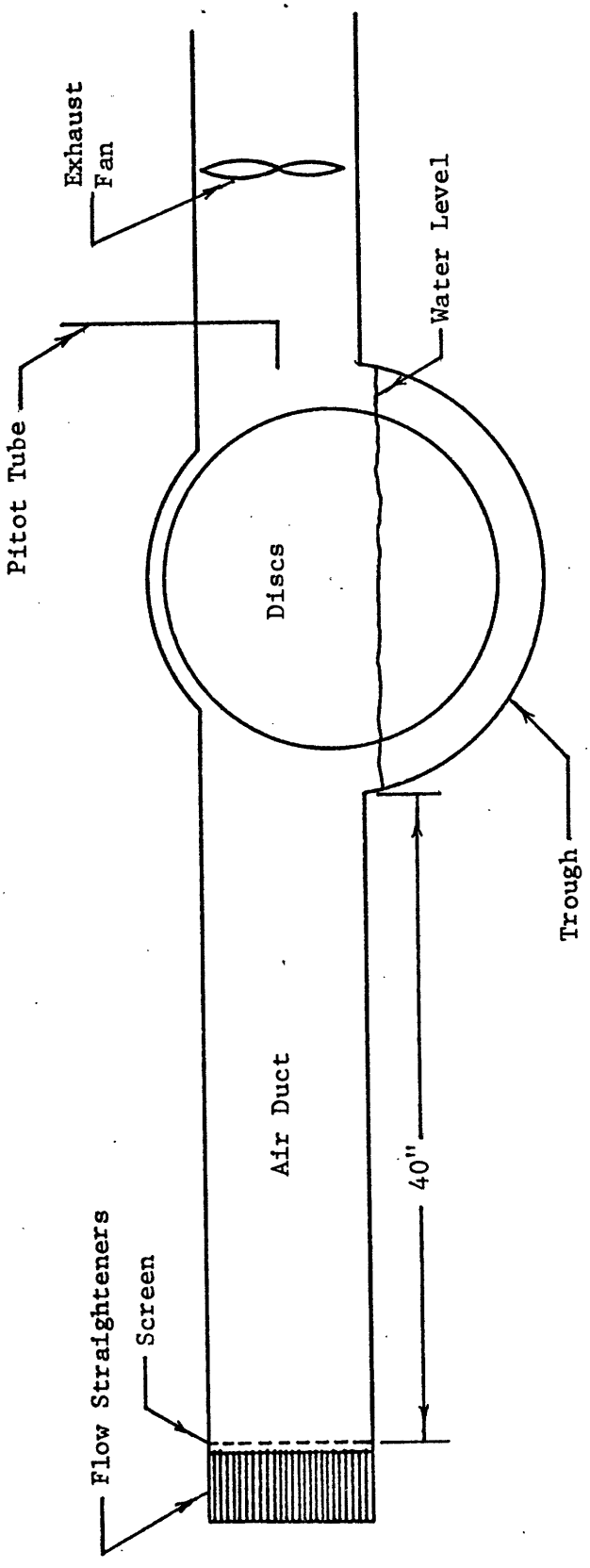

Air Duct - Disc Design

Figure 5

II.2 Flow Visualization Testing

II.2.1 Experiment

15 plates, one of the side plates being made of 0.066 inch thick transparent plexiglas, were mounted on a rotating shaft. The water was fed into the trough through a horizontal pipe with an internal diameter of 1/4 inch. 15 holes 0.081 inch in diameter, spaced 0.33 inch apart, were drilled along the pipe. The water was thus fed into the trough in the form of 15 round jets shooting into the spacings between the rotating plates. The water was pumped out the trough through a 3/4 inch pipe which was located down stream of the rotating plates at the middle of the trough. Figure 6.

To visually observe the flow path occurring between the plexiglass plate and the first steel plate, dye was injected into the jet admitting water between these two plates. Dye was injected by means of a fine 0.028 inch diameter syringe located upstream of the jet. The small amount of dyed solution released from the syringe mixed with water jet, thus making the flow path of the water entering the trough visible through the transparent plexiglass plate.

Test were also run without water circulation. In this case the plates simply rotated in a trough of water. The flowpattern was traced by dyed solution released through a long slender syringe tube of diameter 0.072 inch.

All the flow visualization tests were run with water at room temperature. In the tests with water circulation through the trough, the ratio of the jet exit velocity to the plate circumferential velocity was maintained at a constant value equal to the projected full scale value. This ratio is based on heat transfer requirements. (Appendix (A)). The positions of the water jets were varied in the tests, and the water jets were slightly tilted upward making an angle of roughly 30 degrees with the horizontal.

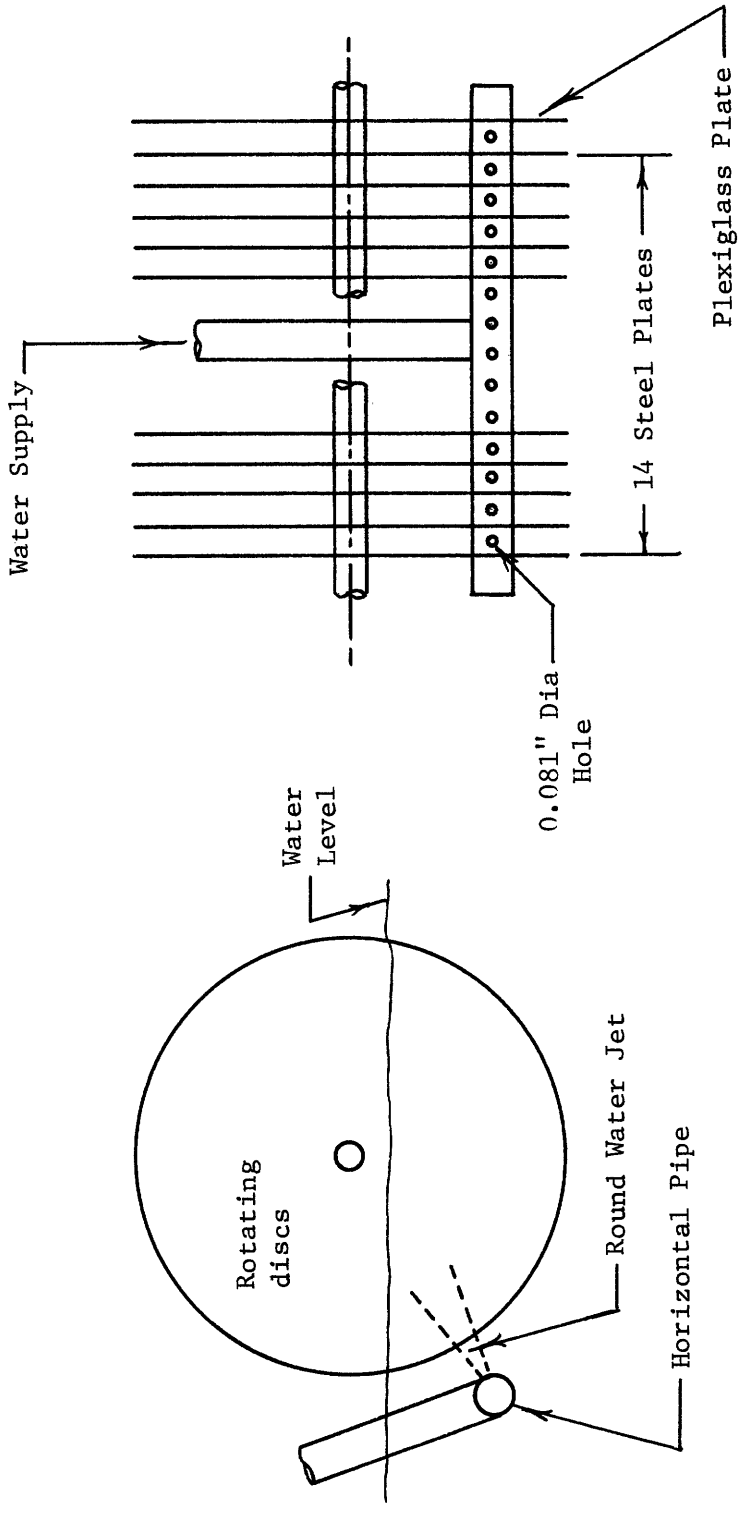

Water Delivery System

Figure 6

II.2.2 RESULTS

The results of the flow visualization tests are shown in the figures 7-11. The arrows in the diagrams indicate the directions of the flow paths.

On examining the results of the flow visualization tests, it appears the flow pattern of the water in the trough is largely determined by the rotating plates. The water jet shoots into the plate spacing only a short distance beyond the plate circumference, then it is carried along by the "currents" generated by the rotating plates. The distance the water jet can travel into the plate spacing is determined by the relative magnitudes of the water jet velocity and the plate circumferential velocity. The water jet velocity decays as the reciprocal of the distance from the jet exit, and at a few inches beyond the plate circumference, the water jet velocity becomes smaller than the plate circumferential velocity. A discussion of the estimate of the distance the water jet can travel into the plate spacing is given in Appendix B.

Figure 7 shows the flow pattern without water circulation through the trough. In general, the flow is circular with the currents following the plate's motion at the perifery of the plate. As there is no water circulation, conservation of mass dictates that somewhere flow must run counter to the direction of the plate rotation. This occurs at shallow depths, where the plate velocity is smaller, and consequently the shear forces are smaller.

Figure 8, the water jet was positioned 3 inches below the water level, and the plates rotated in a direction counter to the water jet. In this configuration, the inflowing water appears to closely follow the currents shown in figure 7. Water exits the jet, rises to the surface, and flows counter to the plates' rotation, and then down to the drain. Two apparent advantages

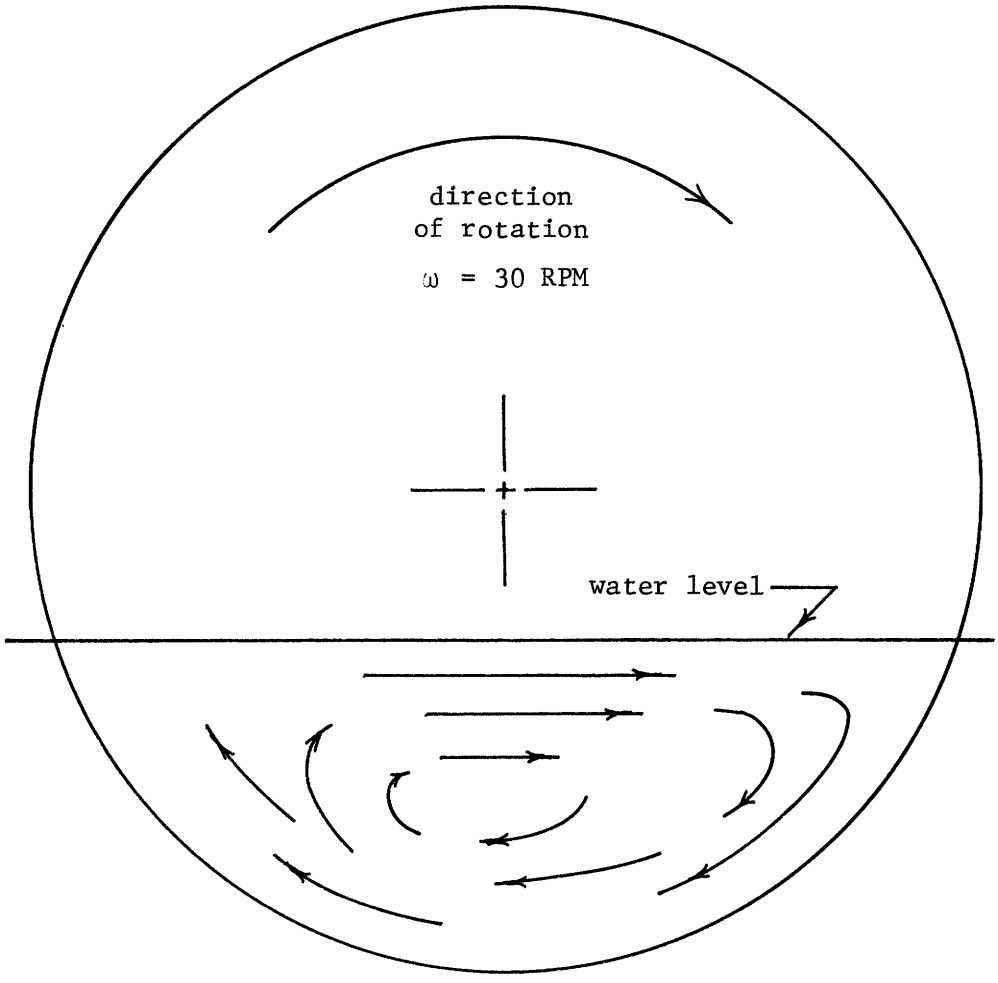

FLOW PATTERN WITHOUT WATER CIRCULATION THROUGH THE TROUGH

Figure 7

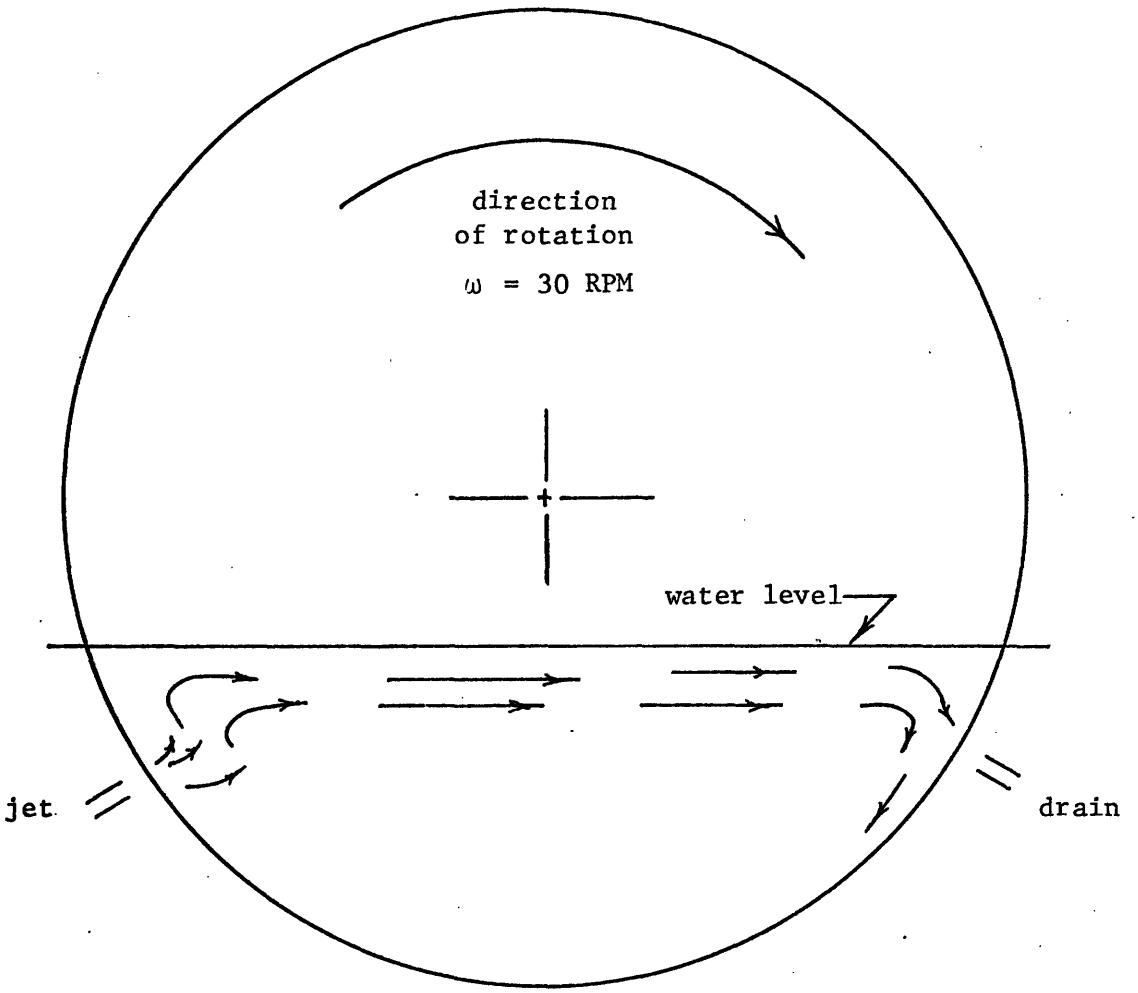

FLOW PATTERN WITH WATER CIRCULATION THROUGH THE TROUGH
Counter flow - with jet 3 inches below water level

Figure 8

to this system are: (1) the plates are heated to the highest temperature possible when they leave the water side since the plates make contact with the hottest water in the last stage during their stay in the water side, and (2) the hot water entering the trough has to travel across the whole diameter of the plate before it arrives at the outlet, thus allowing for a maximum time for heating the plates.

In Figure 9, the water jet was positioned 6 3/4 inches below the water level, and the plates rotated in a direction counter to the water jet. This configuration is similar to that in figure 8. The location of the jet allows the fluid to enter more into the central circular path than in Figure 8. It appears the hot water entering the trough becomes more dispersed and covers a larger surface area of the plates. However, a portion of the hot water entering the trough only travels half of the plate diameter to get to the outlet. As in Figure 8, the discs leave the water immediately after being exposed to the hottest water, but due to the dispersed nature of the water, the temperature may not be as high as in figure 8.

In Figure 10, the water jet was positioned 4 inches below the water level, and the plates rotated in a direction parallel to the water jet. The flow seems to be trapped in some eddy flow not evident from figure 7, with the flow that eventually passes to the drain flowing along the plates' perifery. This configuration has the disadvantage that the plates are not in contact with the bulk of the hottest water just before they leave the water side.

In Figure 11, the water jet was positioned 6 3/4 inches below the water level, and the plates rotated in a direction parallel to the water jet. The fluid is injected at a point far enough below the water level to avoid the eddy of Figure 10, and consequently is swept along the perifery towards the drain. Mixing enroute causes the majority of injected water to pass by the

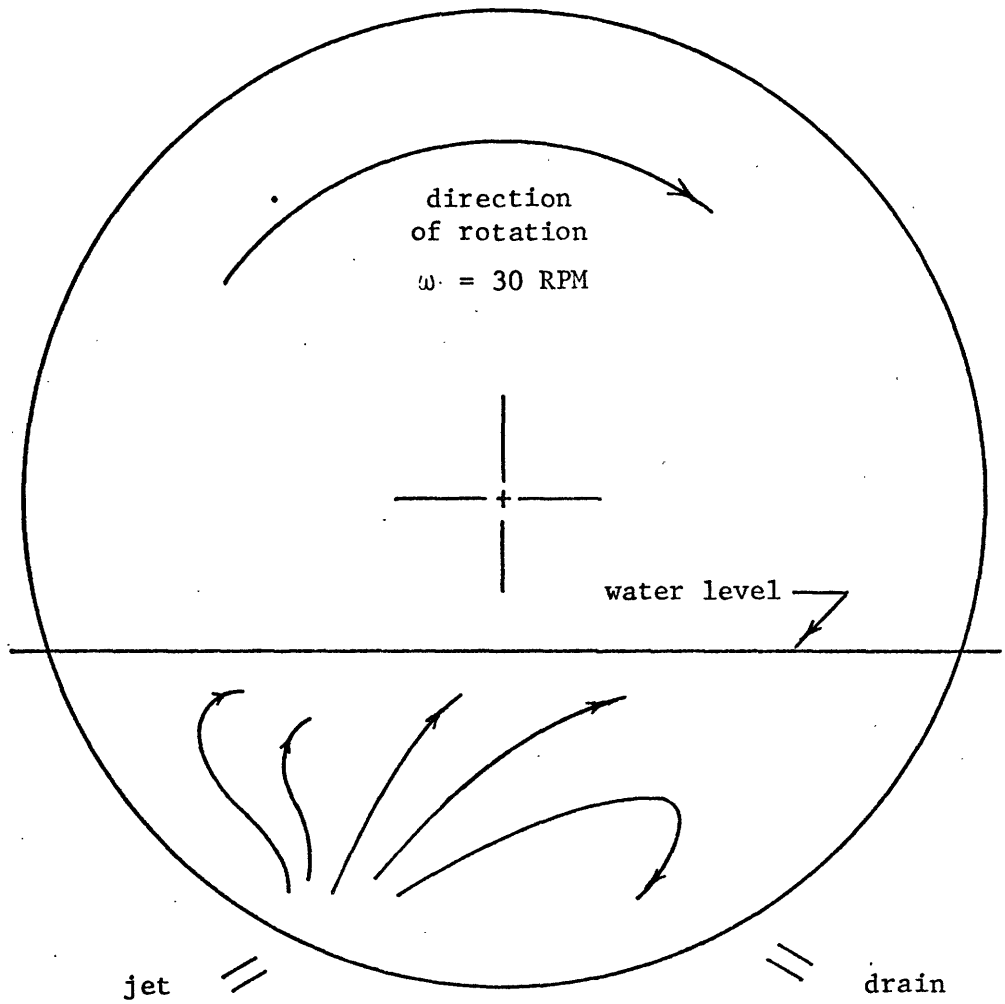

FLOW PATTERN WITH WATER CIRCULATION THROUGH THE TROUGH
Counter flow - with jet 6 3/4 inches below water level

Figure 9

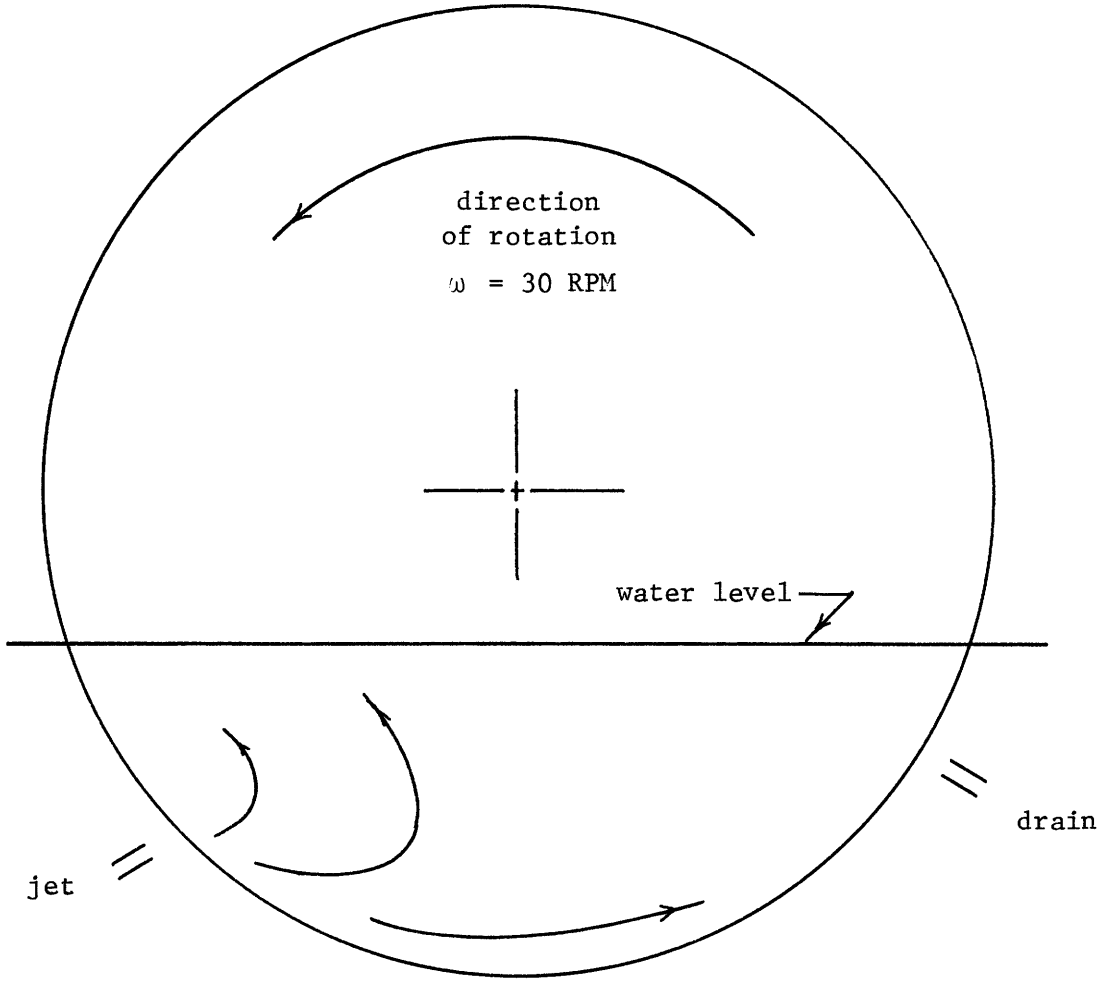

FLOW PATTERN WITH WATER CIRCULATION THROUGH THE TROUGH

Parallel flow - with jet 4 inches below water level

Figure 10

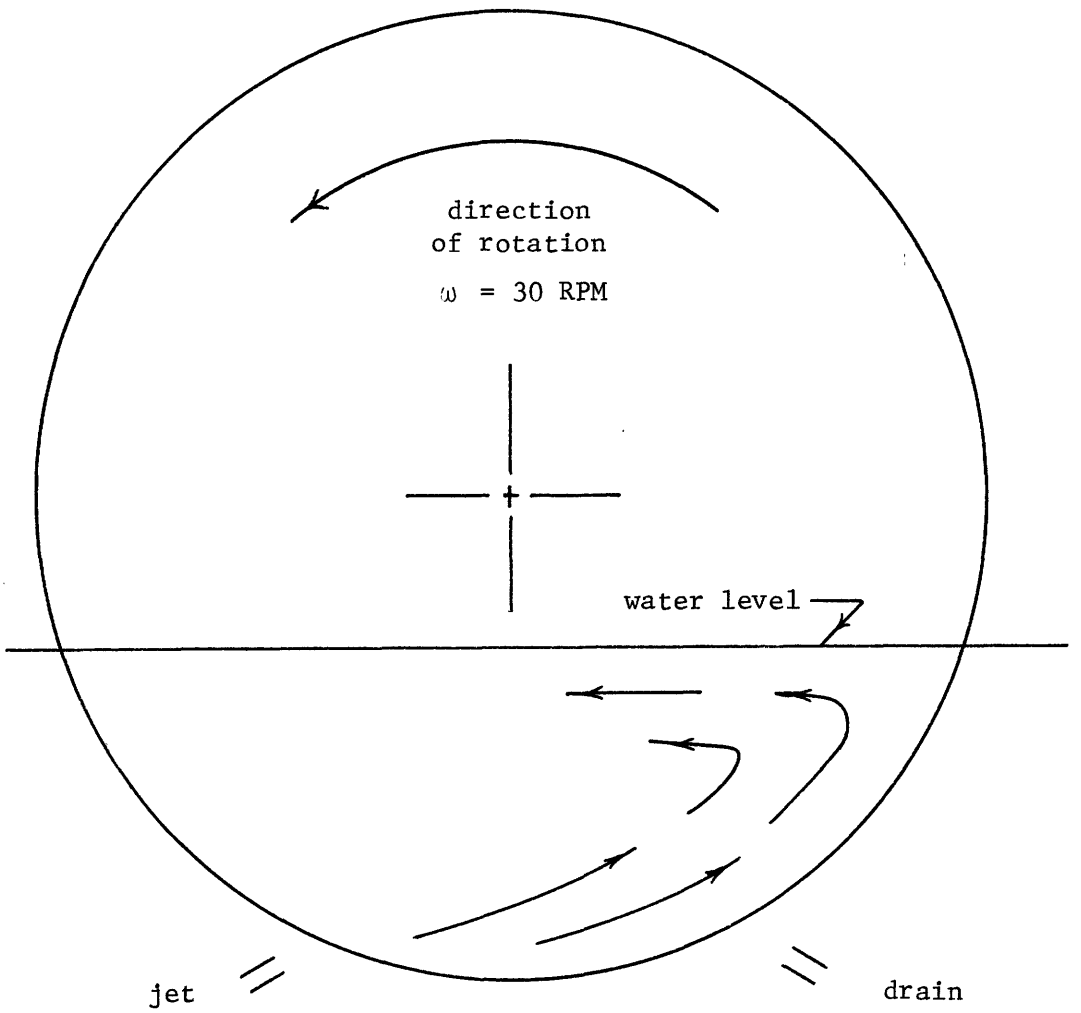

FLOW PATTERN WITH WATER CIRCULATION THROUGH THE TROUGH
Parallel flow - with jet 6 3/4 inches below water level

Figure 11

drain and to recirculate. In a real system, this is tantamount to having a portion of the hot water entering the trough proceeding directly to the outlet without allowing much time for the heating of the plates. Another disadvantage of this system is that the plates are not in contact with the hottest water just prior to entering the air stream.

On comparing these results, the configurations in figure 8 & 9 are superior to these on figure 10 & 11.

As indicated in Section II.2.1, figures 7-11 were drawn by observing the flow of dye injected into the trough with different locations of the water source and different directions of plate rotations. Figures 12-14 are a sequence of photographs following the flow of such an injection for the configuration shown in figure 8. In Figure 12 the dye had just entered the trough at the upper left, and is visible as a dark grey area. The dye, again viewed as a grey area in Figure 13, progresses across the surface of the water towards the drain. Due to mixing, the grey area is more dispersed than in Figure 12. Finally, in Figure 14, the dye reaches the upper right side of the trough by the drain. The overall flow pattern is the same as shown in Figure 8.

Although the tests were run with water at room temperature, it is expected that the same flow patterns will also be observed in the actual case where hot water of about 140°F is fed into the trough containing water of about 135°F. As inertial forces presently dominate, if changes in flow patterns were to occur, it would be as a result of an increased effect of viscous and buoyance forces. The relative magnitude of these forces can be compared by use of dimensionless parameters. The relative values of inertial forces to viscous forces are compared by the Reynold's number, and the relative value of buoyancy to inertial forces is compared by the ratio of the Grashof number to the square of the

PAGES (S) MISSING FROM ORIGINAL

NO PG. 33

Reynold's number (Gr/Re^2).

Inertial to viscous forces: (Re)

where

$Re = \rho V D/\mu$

ρ = density of water = 62.3 lbm/ft^3 @ 60°F

D = hydraulic diameter = 0.66 inch

μ = viscosity of water = 2.71 lbm/hr ft @ 60°F

V = velocity = $R\omega$

R = radius of plate = 10 inches

ω = angular velocity of the plates @ 30 RPM = 60π rad/min

therefore, Re = 12,000.

Thus, at room temperature, the viscous force is negligibly small when compared to the inertia force. Increasing the water temperature from room temperature to 140°F reduces the viscosity of water by approximately half, thereby further reducing the already insignificant viscous force by half. Inertial forces still dominate the viscous forces, and raising the temperature to 140°F will not affect the overall flow patterns.

Bouyancy to inertial forces: (Gr/Re^2)

where

$Gr = g\ B\ L^3\ \Delta T/\nu^2$

Re = 12,000 (from above)

ΔT = temperature variation = 5°F

g = gravitational constant - 32.2 ft/sec^2

B = coefficient of volume expansion - 2.5×10^{-4} at 130°F

L = half of the plate spacing - 0.33 inches

ν = kinematic viscosity of water = 0.022 ft^2/hr at 130°F

therefore

$$Gr/Re^2 = 1.97 \times 10^{-5}$$

The bouyancy force is orders of magnitude smaller than the inertia force. Therefore the buoyance body force due to a 5°F variation in temperature would not affect the flow pattern.

II.3 Selection of Oil

During the initial tests of a small model of the rotary heat exchanger by Robertson [1], it was found necessary to cover the water contained in the trough with a layer of oil to suppress water evaporation. The selection of oil that is used to suppress water evaporation depends on three main factors. As the oil must float on the water, the oil must have a specific gravity less than one. Also it is important that the oil has a negligible evaporation rate. And lastly, the oil film adhering to the plate adds an additional resistance to the plate to air heat transfer. As the added resistance is inversely proportional to the film thickness, it is desirable to have a very low viscosity oil so that the oil film on the plates is very thin. It was suggested by Robertson [1] to use silicone oils as they have a negligibly small evaporation rate. Table I lists 4 silicone oils with relatively low viscosities.

The silicone oils in Table I are manufactured by the General Electric Company. The vapor pressure of high molecular weight silicone oils as measured by Mennicken [2] is shown in Table 2.

When the above data is extrapolated to 135°F, the operating temperature of the silicone oil in the rotary heat exchanger, the vapor pressure is approximately 10^{-8} torr. With a vapor pressure of 10^{-8} torr, an estimate of the oil evaporation rate by the method suggest by Robertson [1] for a 1000 MW power plant shows an insignificant 3 lbm/hr. It thus appears that the silicone oils satisfy the negligible evaporation requirement. All the 4 silicone oils mentioned have specific gravity less than one. The thermal resistance due to the film of silicone oil on the rotating plates can be estimated (see reference 1), and its effect on the heat transfer of the rotary heat exchanger will be tested.

Another problem encountered during the tests of a small model of the rotary heat exchanger by Robertson [1] is that as the plates rotate at high speed, they churn the oil layer into the water causing a very thorough mixing of the oil with the water. The commercial name of the oil used by Robertson [1] is Rubrex 100, manufactured by the Mobil Oil Company.

Tests were run with the silicone oils SF-96 and SF-1147 to study the churning effect of the rotating plates. With R = radius of plate = 10 inches

ω = angular velocity = 20 r.p.m.

D = plate spacing = 0.33 inch

TABLE 1

Commercial Names	Nominal viscosity (centistokes) at 25 C	Specific gravity at 25 C
SF-96	20	0.953
SF-1147	50	0.890
SF-96	50	0.963
SF-81	50	0.972

TABLE 2

Temperature C	Vapor pressure (torr)
140	1×10^{-5}
170	1×10^{-4}
200	8×10^{-4}

no thorough mixing of the silicone oil and the water was observed. The motion of the fluids in the trough brought about by the rotating plates was, however, quite violent. Yet the silicone oil stayed as a separate layer on top of the water, with drops of silicone oil moving up and down just beneath the layer of silicone oil.

III. Disc Ribbing - Roughened Surfaces

III.1 Introduction

According to previous studies [1,3,4] on dry cooling towers for large scale electrical power plants, the periodic cooling tower holds an economic advantage over the conventional dry tower. A computer model was developed to design the heat exchanger configuration resulting in the lowest total incremental and capital cost for a periodic tower with given power generation, turbine heat rate versus back pressure performance, cost data and plate diameter. The heat transfer and cost equations may be reduced to five independent variables which must be optimized: (1) D - the distance between plates, (ft); (2) T_D - the design ambient air temperature, or the ambient air temperature at which the power plant can deliver its fully rated power, (°F); (3) T_{hl} - the inlet water temperature to the tower, (°F), (4) V_A - the air velocity through the tower, (ft/hr); and (5) V_W - the water velocity through the tower, (ft/hr).

Since more than half of the total cost of a dry tower is the cost of the heat transfer surface, a reduction in the required heat transfer surface area significantly lowers the capital cost. For a given heat rejection rate and temperature difference between hot water and cold air, an increase in the surface heat transfer coefficient reduces the total heat transfer area needed. One method to improve the thermal performance of a heat exchanger for a constant pumping power is to roughen the surfaces of the heat exchanger. To take into account the surface roughness effect on the cost of periodic cooling tower, the existing optimum design program was modified by increasing the number of independent variables from five to eight. These additional three variables are: (1) DIA - diameter of the plates (ft); (2) E/D - ratio of the height of the ribs to the spaces between the plates; (3) P/E - ratio of the space between the ribs to the height of the ribs.

According to the eight variable optimization, the lowest capital and incremental cost will be obtained when the rib heights are 0.016" and the diameter of the plates are 2 feet. These dimensions are impractical, however, because the thickness of the oil layer covering the plates is greater than the rib height. Therefore, because of the oil layer, the surface appears as a smooth surface. Sensitivity studies of the influence of the rough surface on the cost was accomplished by using different rib heights and different spacings between

the ribs such that the thickness of the oil layer is very much less than the heights of the ribs. Under these conditions, a specific roughened surface (E/D = 0.08, P/E = 10) yields a 15 - 20% saving of capital and incremental cost over a smooth surface. In both cases, the disc diameter is five feet, and the analysis included the effect of the oil layer. These results illustrate the economic advantages of the roughened surface over the smooth surface.

III.2 Modification of Optimum Computer Design Program

According to a literature survey, the rough surface has a better thermal performance than that of a smooth surface for a given pumping power. One of the methods to roughen the smooth surface is to fasten or fabricate ribs of a specific shape on the smooth surface heat exchanger [5,6]. The main purpose of ribs on the smooth surface is to break down the laminar sublayer of turbulent flow, thereby inducing more turbulence near the wall of the heat transfer surface. This effect will increase both the heat transfer coefficient and the friction factor.

The most important parameters of a rib-rough surface which influence the heat transfer coefficient and friction factor for a given flow conditions are the height of the ribs and the space between the ribs. In the optimized design program for the rough surface periodic heat exchanger, these values are included in the model as E/D and P/E (see fig. 15) where,

$$\frac{E}{D} = \frac{\text{the height of the ribs}}{\text{the space between plates}},$$

$$\frac{P}{E} = \frac{\text{the space between ribs}}{\text{the height of the ribs}}$$

One of the suggested methods to roughen the circular periodic heat exchanger surfaces is to have square-ribs in radial directions on smooth surfaces (see figure 16). In this radial-type of square-rib rough surface, the space between the ribs (i.e. P) varies from the center to the edge of the circle and the flow attack angle varies from 0° to 180° (see figure 16).

The effect of E/D and P/E on the heat transfer coefficient and friction factor for internal flows has been investigated quite extensively, but not on the geometry and flow conditions as would be used on the periodic heat exchanger. Before more accurate experimental data can be determined for roughened geometries similar to that proposed for the periodic heat exchanger, it

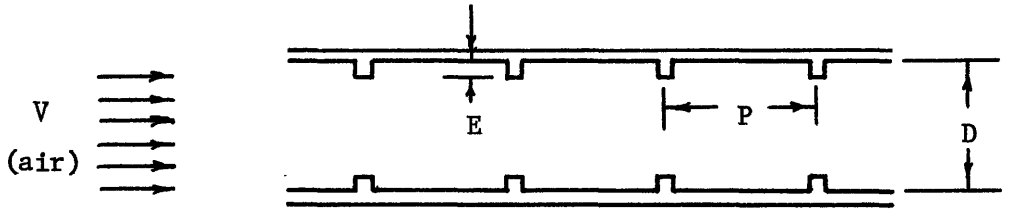

Square-Ribs of Rough Surface between Parallel Plates

Figure 15

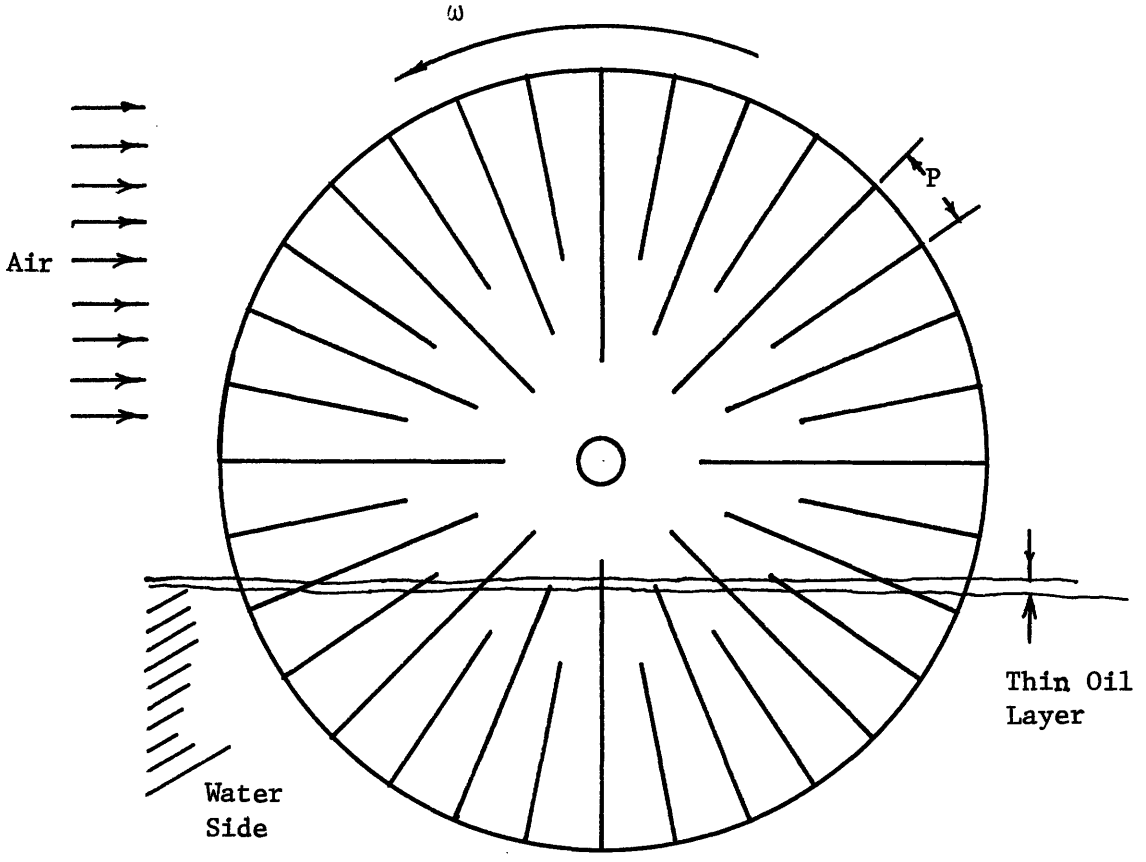

Square Ribs in Radial Direction on Smooth Surfaces

Figure 16

is still useful to predict approximate results using previous investigators results. The following existing correlation [5] were used to predict the heat transfer coefficient and friction factor for periodic heat exchanger performance. It must be noted that the following correlations hold for transverse ribs only. Since in the rotary tower the angle between the rib and the flow direction is constantly changing, the use of this correlation is not strictly correct.

$$St = \frac{f/2}{1 + \sqrt{f/2}\,[4.5\,(e^{+})^{0.28}]\,Pr^{0.57} - 0.95\,(P/E)^{0.53}}$$

$$\sqrt{2/f} = 2.5\,\ln\,(D/2E) - 3.75 + 0.95\,(P/E)^{0.53} \qquad (1)$$

$$e^{+} = (E/E)\,Re\sqrt{f/2}$$

where

St = Stanton number

Re = Dv/μ Reynolds number

D = Diameter of circular tube

f = Friction factor

Pr = Prandtl number, evaluated at T_{av}

T_{av} = Mixed mean fluid temperature

V = Average fluid velocity

E = Height of ribs

P = Space between ribs

The above correlations are suitable under the following conditions: $e^{+} > 30$, P = constant, $E/D \simeq 0.01\text{-}0.04$, $P/E \simeq 10\text{-}40$, $Re \simeq 10^{4}\text{-}10^{5}$, $Pr \simeq 0.71\text{-}37.6$, flow attack angle = 90°, and was experimentally determined for internally finning tubes.

It should be pointed out for the case of a smooth surface, the Stanton number is a function of Re and Pr only. For the rough surface case the Stanton number is a function of Re, Pr, E/D and P/E. That means E/D and P/E must be independent variables in the optimum design program as values of E/D and P/E

affect the heat transfer, and hence, in turn affect the capital and incremental cost for periodic heat exchanger. In addition, in last year's Annual Report, it was assumed that the largest plate diameter (DIA = 5 ft) would have the best thermal performance [1]. This may not be the case for square-rib rough surface heat exchanger. The plate diameter must be allowed to vary as the whole system is optimized. Hence, the optimum design program for the periodic cooling tower was modified by increasing the number of variables from five (T_D, T_{hl}, D, V_A, V_W) to eight (T_D, T_{hl}, D, V_A, V_W, E/D, P/E, DIA).

In the earlier report [1], the water side piping cost from the turbine to the cooling tower and the land cost of cooling tower area were not included. In order to prevent three or four more variables from entering the program's minimization procedure, the following approximate method was used to calculate pressure drop from the turbine to the cooling tower and the cost of the associated piping. This method is similar to that used in part I of last year's annual report.

Using the definition of friction factor, the pressure drop through one pipe from the turbine to the tower is:

$$\Delta P_{pipe} = 4f \frac{L}{D_p} \frac{G^2}{2 \rho g_o} \tag{2}$$

For the total pressure drop, this must be multiplied by both the number of pipes running from the turbine to the tower, and by 2 (to allow for the return flow to the power plant). Hence

$$\Delta P_{tot\ pipe} = 2\ N\ \Delta P_{pipe} \tag{3}$$

where, in the above equations,

G = mass flow rate per pipe, or W/NA

W = flow rate for the system

N = number of pipes from the turbine to the tower

A = flow area of one tube, $\pi D_p^2/4$

L = length of the pipe

D_p = diameter of the pipe

g_o = constant: 4×10^8 lbm-ft/lbf-hr^2

ρ = density of water, 62 lbm/ft^3

μ = viscosity of water, 1.6 lbm/hr-ft

With the approximate relation that

$$f = 0.46/Re^{0.2} \tag{4}$$

where

$$Re = \frac{W D_p}{N A \mu} = \frac{4 \quad W}{\pi D_p \mu N} \tag{5}$$

the total pressure drop becomes

$$\Delta P_{tot\ pipe} = 0.368\ N\ (\frac{\pi}{4}\ \mu D_p)^{0.2}\ (\frac{4}{\pi}\ \frac{1}{D_p^2})^2\ \frac{L}{D_p}\ \frac{W^{1.8}}{N^{0.8}} \tag{6}$$

$$\Delta P_{tot\ pipe} = \text{function of } (D_p, \frac{L}{D_p}, W, N)$$

In order to simplify the relation, assume D_p = 8ft (and costs 173 \$/ft), and $L/D_p = 5$. Then

$$\Delta P_{tot\ pipe} = \text{function of } (W,N)$$

and the cost for the piping is:

$$\text{Cost} = 2\ N\ L(173) = 1.384 \times 10^4\ N \text{ Dollars} \tag{7}$$

From the above expressions, an increase in the number of tubes (N) will result in decreasing ΔP and Re, and increasing the cost of the tubes. For a reasonable periodic cooling tower water flow rate ($\omega = 10^8 - 10^9$ lbm/hr) and a reasonable Reynolds number ($Re \simeq 10^5$) in the ducting, it was assumed that this number of ducts (N) is equal to 10^2, then

$$\Delta P_{total} = 2.2 \times 10^{-16}\ \omega^{1.8}\ \text{PSF} \tag{8}$$

and the cost of the ducting = $\$1.384 \times 10^6$

These two values were included in the eight variables aptimum design program for the rough surface periodic cooling tower. To account for land costs, it is assumed that

$$\text{Land Cost} = \text{Land Area} \times \text{Land Cost per ft}^2$$
$$= (D\ N\ DIA) \times \text{Land Cost per ft}^2.$$

For an approximation, assume that D = 1", $N = 10^6$, DIA = 5 ft, and land cost per ft^2 = 0.226 $/ft^2$, then land cost = $\$10^5$. This value is small when compared with the capital cost. Using the existing input cost data [1] and the above modified eight variable optimum design program, the results as listed in Table 3 have been obtained.

TABLE 3

8 variables: (T_D, T_{hl}, D, V_A, V_W, E/D, P/E, DIA)

Results: DIA = 2.04 ft

D = 0.36 in

E/D = 0.045

P/E = 5.15

E = 0.016 in

P = 0.08 in

V_A = 16.452 fps

h = 16.3 BTU/hr ft^2

CAPIT = 13.2×10^6 dollars

INCREM = 0.374 mills/kw hr

$Re_{air} = 0.546 \times 10^4$

$N = 5.27 \times 10^6$

Q_{plat} = 994

Eff_A = 0.775

Eff_W = 0.178

Δp = 4

Surf = 0.4

T_D = 75°F

III.3 Oil Thickness Consideration

The method to prevent the water from evaporating in the periodic heat exchanger is to use a thin oil layer floating on the water surface. The oil will preferentially adhere on the heat exchanger surface when it rotates from the hot water to the cold air stream. The thickness of the oil layer on the heat exchanger surface will influence the heat transfer performance. Levich [7] gives an equation for the thickness of a liquid coating on a solid withdrawn from a liquid as,

$$\delta_o = \left(\frac{\mu V}{\rho g}\right)^{1/2} f\left(\frac{\mu V}{\sigma}\right) \tag{9}$$

with

$$f\left(\frac{\mu V}{\sigma}\right) = 0.93 \left(\frac{\mu V}{\sigma}\right)^{1/6} \quad \text{for } \frac{\mu V}{\sigma} < 1$$

and $f\left(\frac{\mu V}{\sigma}\right) = 1 \quad \text{for } \frac{\mu V}{\sigma} \gg 1$

where

σ = surface tension, dynes

V = velocity of solid withdrawal rate from liquid, cm/sec

ρ = coating thickness density, $g\,m/cm^3$

δ = coating thickness, cm

μ = viscosity, poise

Assuming that the above equations can apply to the rough surface periodic heat exchanger, the maximum thickness at the outer edge of the circular plate is 0.023" (for DIA = 2.04, ω= 10 RPM, & Silicon oil). The minimum oil thickness (at $r = r_o$) is 0.0126". The oil thickness between r_o and R is almost a parabolic distribution (see figure 17). To simplify the problem, assume the oil thickness between r_o and R is a linear distribution. As the oil seems to flow over the entire surface area, it is reasonable to calculate the average coating oil thickness based on the total surface area. Hence,

$$\delta_{avg} = 1/2(\delta_{@R} + \delta_{@r_o})\ (\pi R^2 - \pi r_o^2)/\pi R^2 \tag{10}$$

for the case of $R = \frac{2.04}{2}$ ft, $r_o = \frac{1}{33} R$, then δ_{avg} = 0.0162 in.

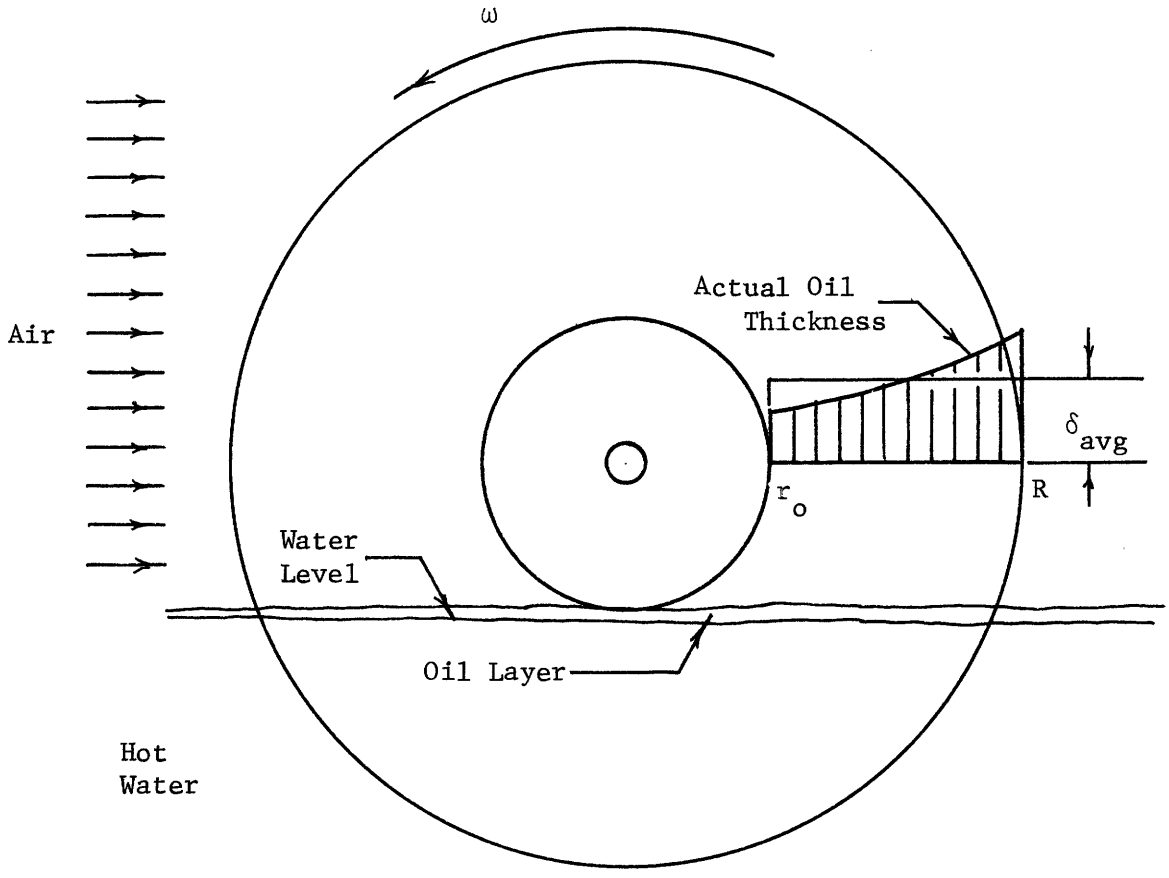

Oil Thickness on the Rotating Surface

Figure 17

From the eight variables optimum design program, the optimum plate diameter is 2.04 ft and the rib height is 0.016 in. From the above approximate oil thickness calculation, the average oil thickness over the rough surface is 0.0162". Obviously, the coating oil thickness will cover the ribs on the surface, and the surface roughness effects are almost reduced to zero. Also because in this optimized case the height of the ribs and the space between ribs are dimensionally small, it would be difficult or expensive to produce the ribs in a manufacturing process. In addition, the Reynolds number is just near the transition region, where the accuracy of the correlation [5] to predict the Stanton number and friction factor for the case of rough surface periodic heat exchanger is questionable. Even though the 2 ft diameter heat exchanger provides the lowest capial and incremental cost for the rough periodic heat exchanger, it is impractical due to the above disadvantages.

In order to make the periodic cooling towers more practical, it is important to study the sensitivity of roughness on the capital and incremental cost. The problem considered here is not only on the point of view of economic advantage but also on the reality of manufacturing processes of the roughened periodic heat exchanger. Different optimum designs were achieved by changing the height of ribs and the space between ribs for fixed plate diameter. The results of these sensitivity studies are shown on figures 18, 19, and 20.

In figures 18 and 19 capital and incremental costs are plotted against design temperature for the cases where P/E is varied from 10 to 60, and E/D is either 0.01 or 0.08. The optimum case occuring when P/E = 10 and E/D= 0.08. If one further decreases P/E and increases E/D, the capital and incremental cost will increase again (this effect is not on these figures). In figure 20, the effect of increasing the disc diameter from 2 ft to 5 ft is illustrated. There is a 5% increase in the incremental and capital cost by increasing the diameter from 2 to 5 feet, however, as noted before, the 5' diameter plate is more practical For the optimized 5' diameter plates, E = 0.09" and P = 0.52", and coating oil thickness, δ = 0.0164".

Figure 21 and Table 4 are the cost comparison between a rough and smooth surface periodic heat exchanger when taking into account the effect of the coating oil thickness. For a specific square-rib rough periodic heat exchanger (E = 0.07", P = 0.7") using 5' diameter plates, there is a 15 - 20% savings on capital and incremental cost over smooth surface periodic heat exchanger when taking into account the coating oil thickness.

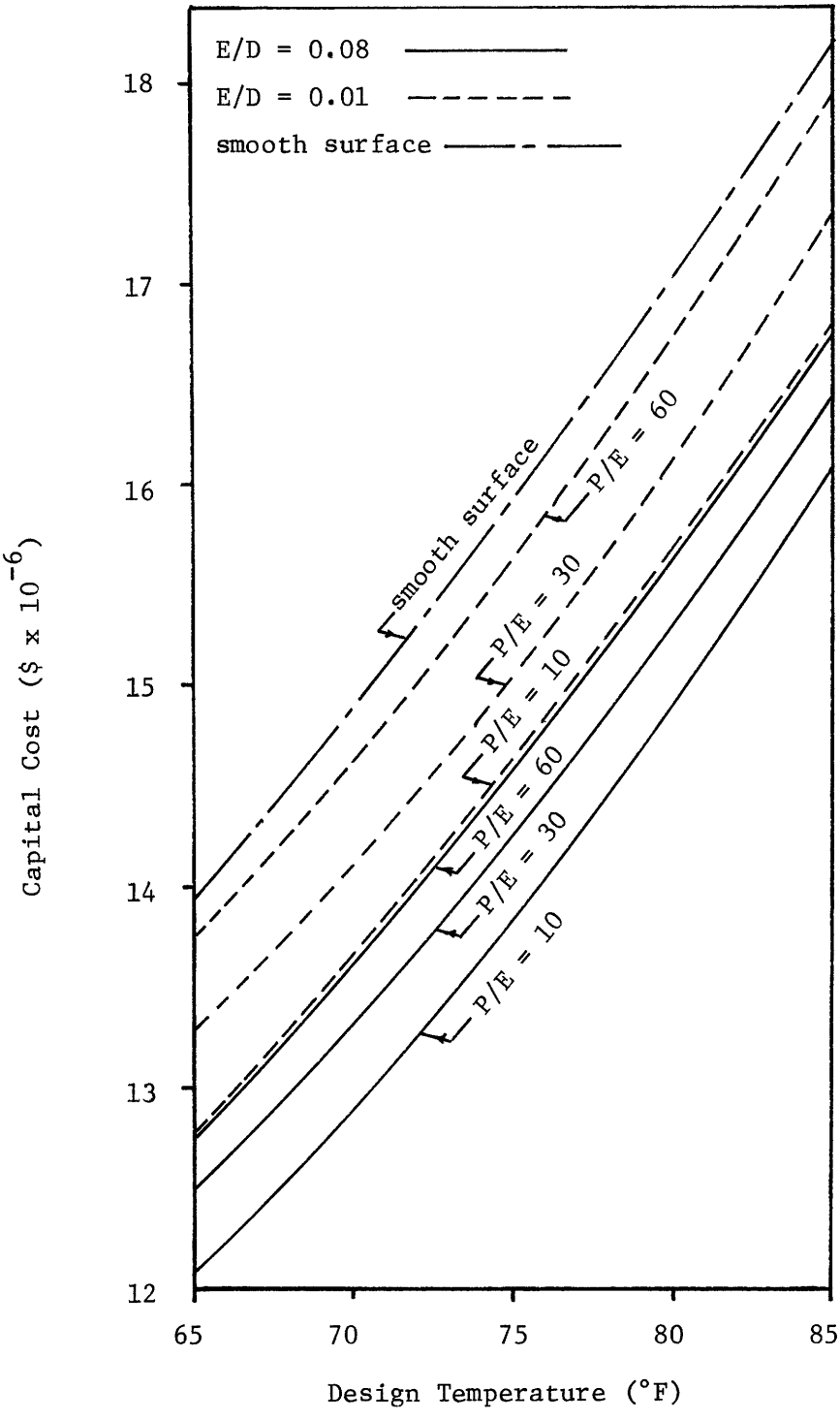

CAPITAL COST VS. DESIGN TEMPERATURE
for smooth and various
roughened surfaces

Figure 18

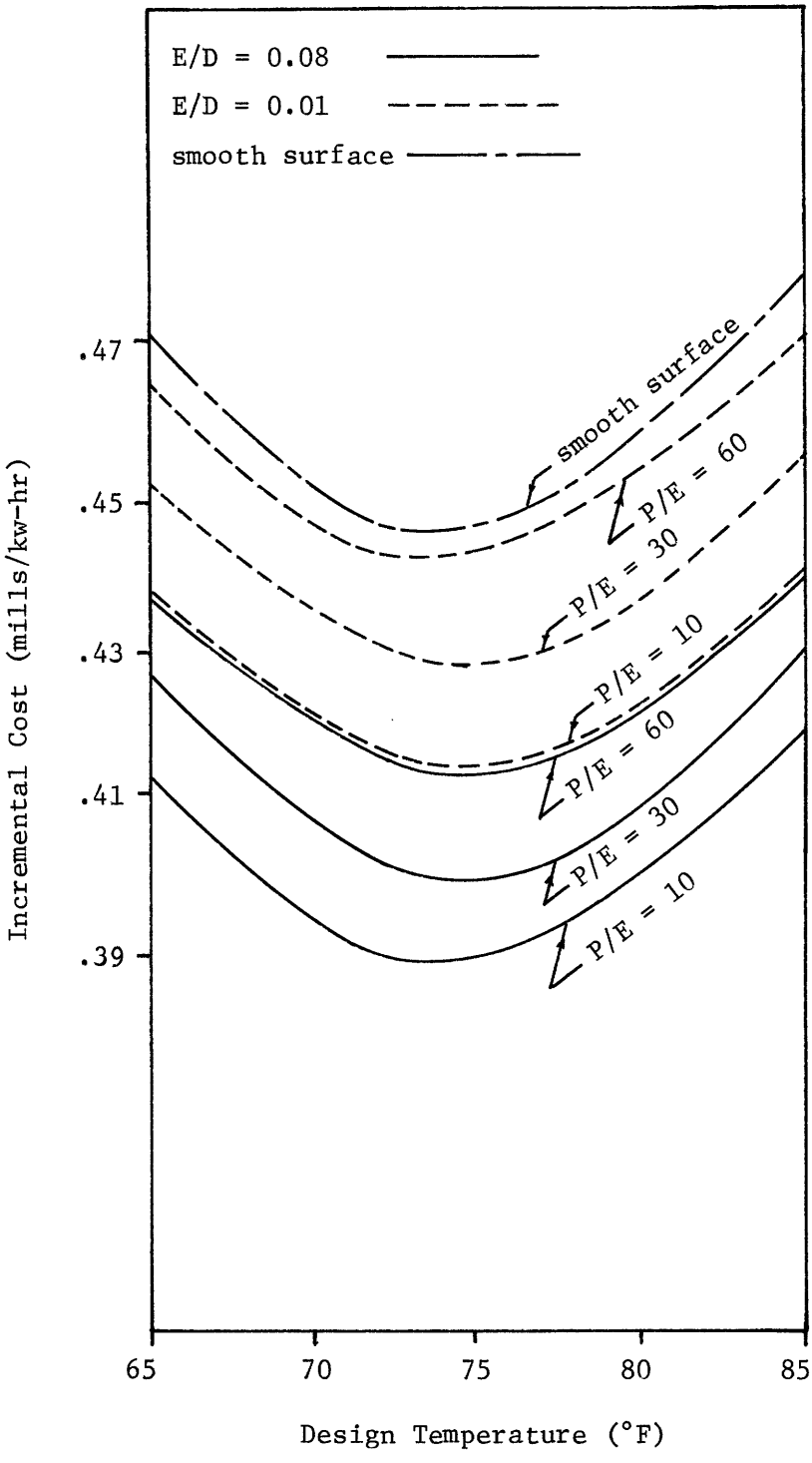

INCREMENTAL COST VS. DESIGN TEMPERATURE
for smooth and various
roughened surfaces

Figure 19

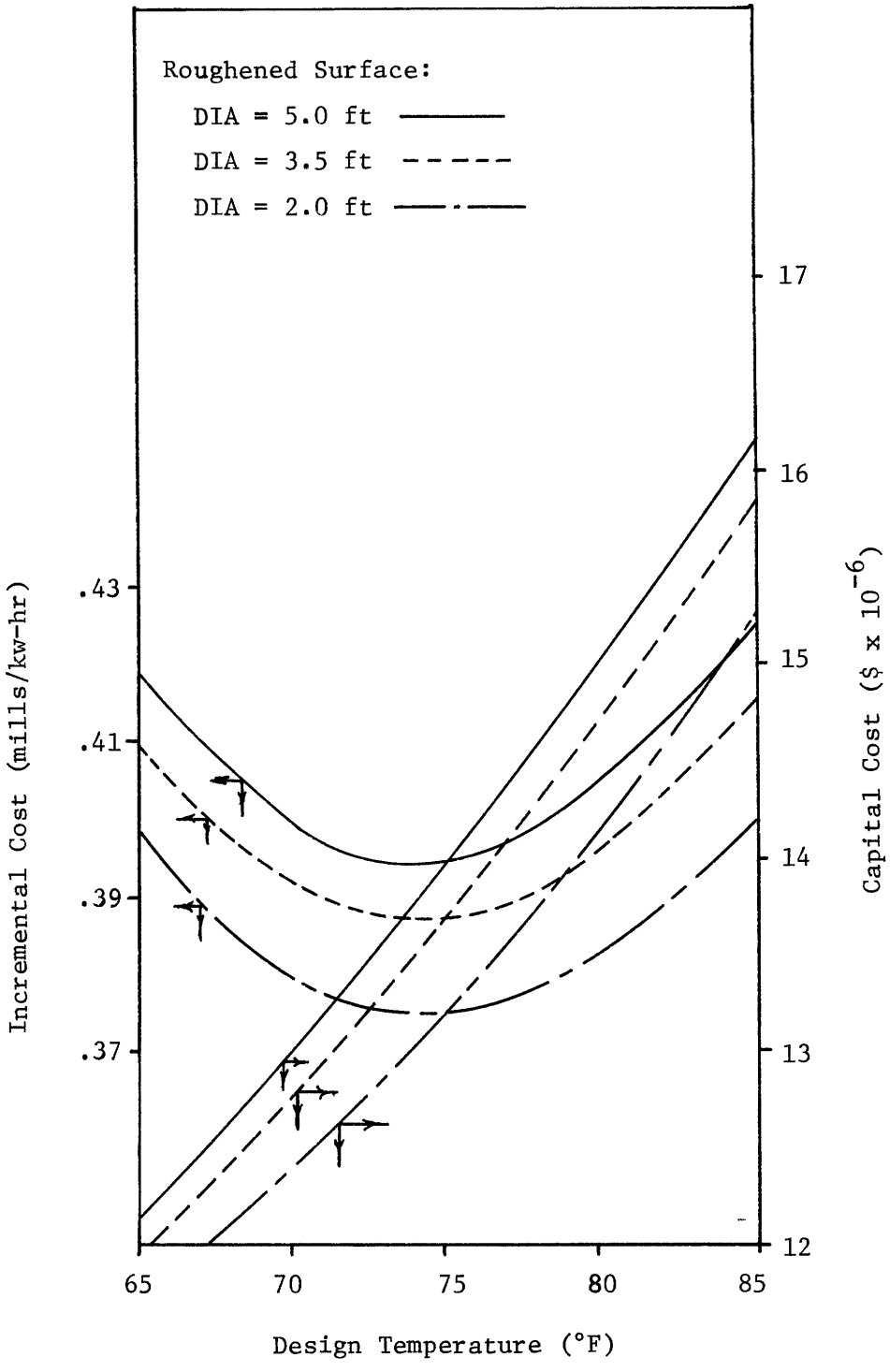

INCREMENTAL AND CAPITAL COSTS VS. DESIGN TEMPERATURE
for different diameter roughened plates

Figure 20

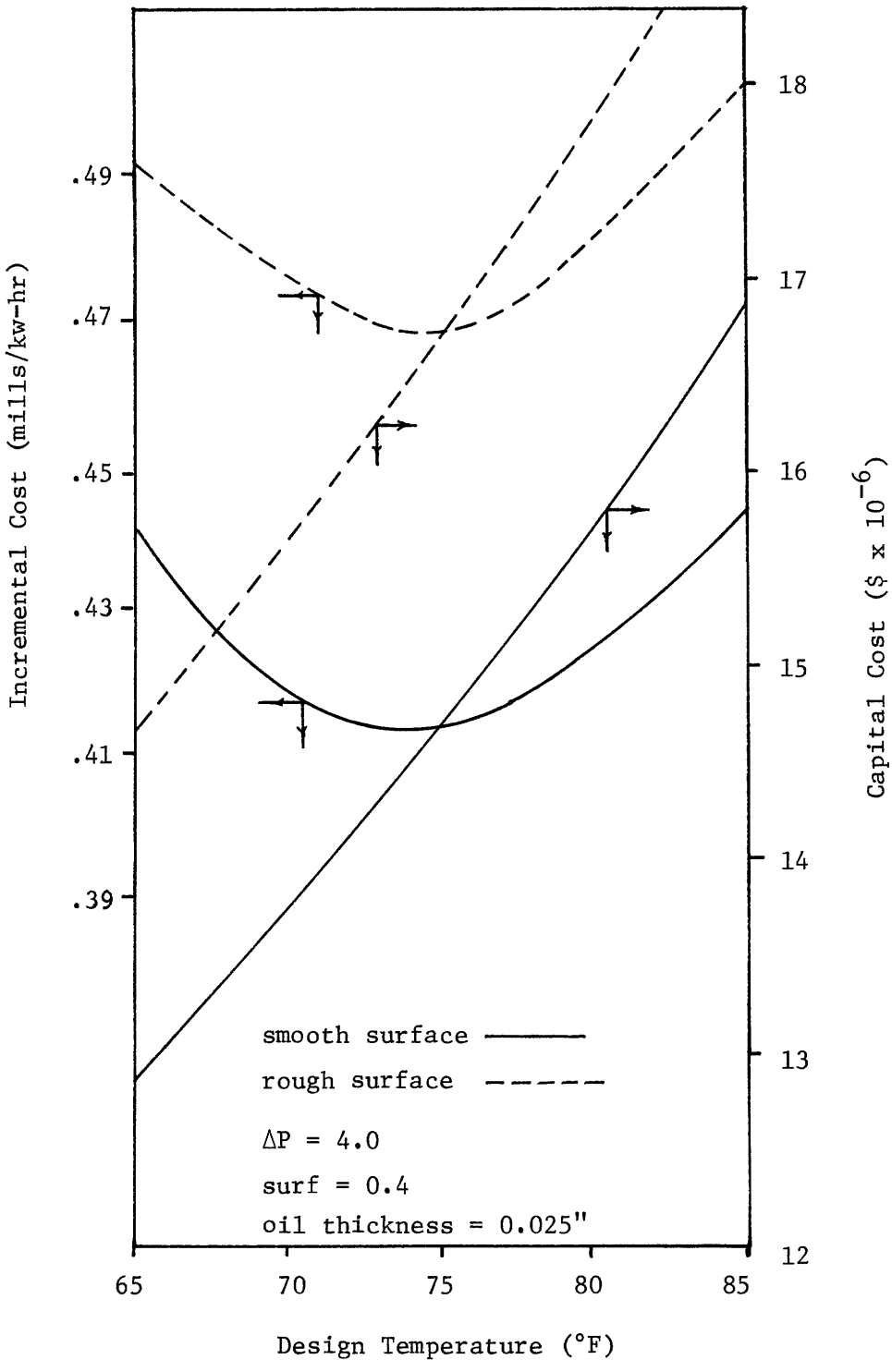

INCREMENTAL AND CAPITAL COSTS VS. DESIGN TEMPERATURE
for smooth and roughened plates

Figure 21

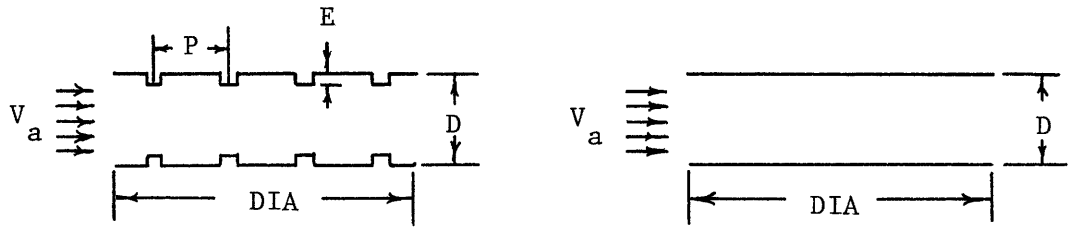

Rough Surface

Smooth Surface

TABLE 4

No Oil Thickness	Oil Thickness = 0.025"	No Oil Thickness	Oil Thickness = 0.025"
DIA = 5 ft	DIA = 5 ft	DIA = 5 ft	DIA = 5 ft
V_A = 14.5 fps	V_A = 13.5 fps	V_A = 37.6 fts	V_A = 36.5 fps
h = 12.5	h = 10.1	h = 10.2	h = 8.5
D = 1"	D = 0.9"	D = 0.366"	D = 0.35"
surf = .4	surf = .4	surf = .4	surf = .4
Δp = 4	Δp = 4	Δp = 4	Δp = 4
V_W = .081 fps	V_W = 0.054 fps	V_W = .085 fps	V_W = .085 fps
T_D = 75°F	T_D = 75°F	T_D = 75°F	T_D = 75°F
T_W = 128°F	T_W = 128°F	T_W = 127°F	T_W = 127°F
Q_{plat} = 5730	Q_{plat} = 4940	Q_{plat} = 5194	Q_{plat} = 4790
N_{plat} = 0.916×10^6	N_{plat} = 1.06×10^6	N_{plat} = 1.01×10^6	N_{plat} = 1.1×10^6
Eff_A = 0.688	Eff_A = 0.685	Eff_A = 0.637	Eff_A = 0.598
Eff_W = 0.14	Eff_W = 0.225	Eff_W = 0.321	Eff_W = 0.331
CAPIT = 13.75×10^6	CAPIT = 14.64×10^6	CAPIT = 15.85×10^6	CAPIT = 16.64×10^6
INCREM = 0.39	INCREM = 0.416	INCREM = 0.448	INCREM = 0.472
E/D = 0.08	E/D = 0.08		
E = 0.08"	E = 0.07"		
P/E = 10	P/E = 10		
P = 0.8"	P = 0.7"		

IV. FULL SCALE MODEL

The size of the full scale rotating discs to be used in this model was limited by the width of the largest strip of sheetmetal commercially available, five feet. Using a five foot disc of 22 gauge sheetmetal as the basic building block of the unit, design work was concentracted on providing a facility which could evaluate the performance of this model and the fabrication of the discs. This full scale model will provide for research into such anticipated problems as the structural integrity of a hortizontal row of closely spaced five foot diameter discs, associated vibration problems, bearings and optimum horsepower requirements for rotating the discs at different speeds, and baffling for obtaining uniform air and water velocities across the discs.

IV.1. CONCEPTUAL FACILITY DESIGNS

A study was made to determine the type of testing facility to be constructed. Three basic types were considered. These were the closed loop circuit with cooling (Figure 22), open circuit with cooling (Figure 23), and the open circuit with no cooling (Figure 24).

IV.1.1. CLOSED LOOP CIRCUIT WITH COOLING

The advantage of the loop system shown in Figure 22 is that little if any air temperature change occurs outside the system when it is operated. This is because the air inside the loop is repeatedly heated and cooled with only insignificant amounts of make-up air added to the

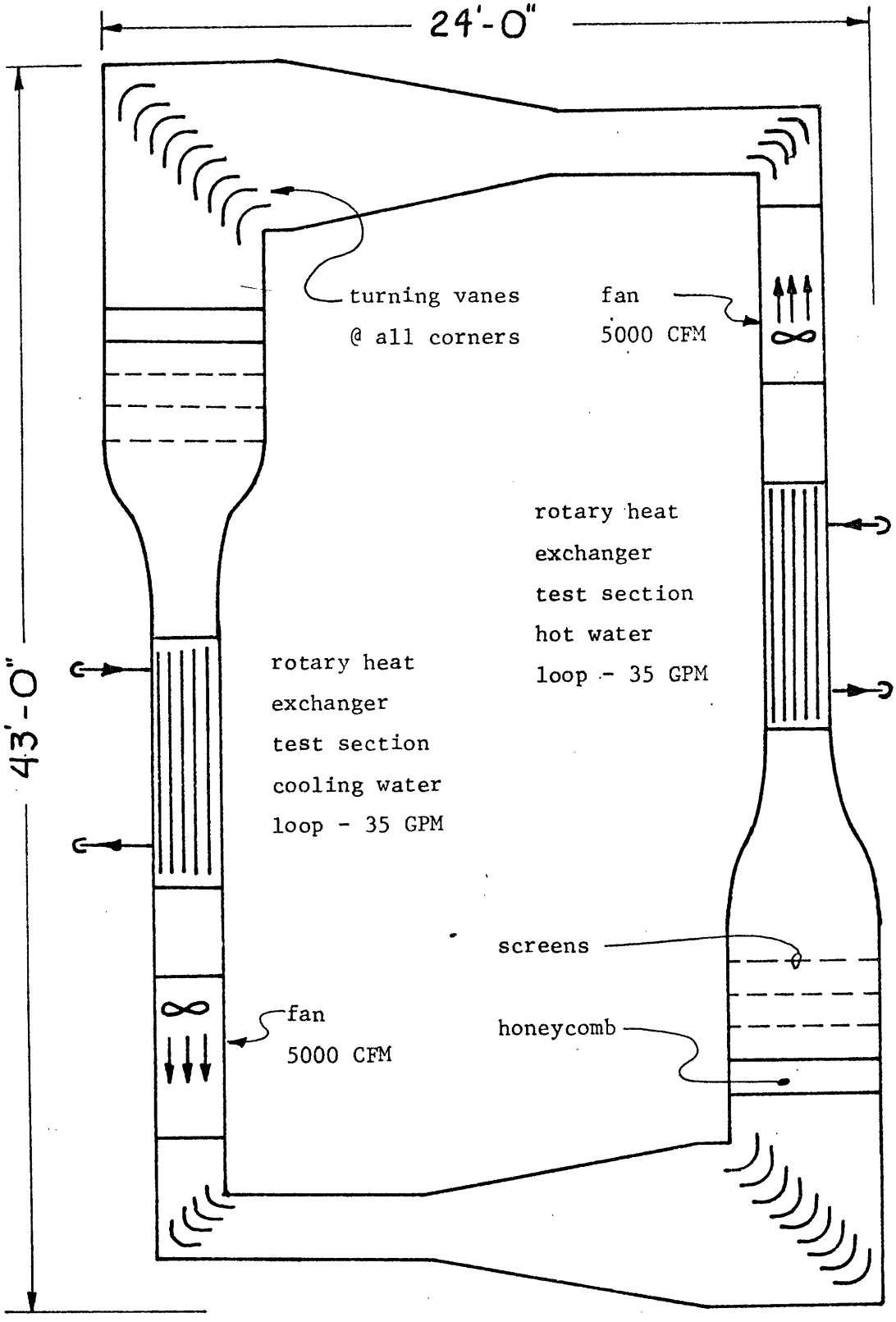

Closed circuit loop with cooling - Figure 22

system. The air in the system will adjust its average temperature so that the heat added to it in the periodic heat exchanger section plus the heat energy from the circulating fans equals the heat removed from it in the cooling periodic heat exchanger section plus the heat losses in the circulating loop. This system allows the equipment to be run in a laboratory next to other experiments with minimum interference. The disadvantage to such a system is that by its very design it involves twice the room and expense as does the open circuit type, and steady state conditions would be obtained only after a lengthly warm up time.

IV.1.2 OPEN CIRCUIT WITH COOLING

The open circuit system with additional air cooling coils shown in Figure 23 represents the minimum apparatus which would allow the experiment to be operated in a laboratory occupied by other experiments, assuming that the systems air inlet and outlet velocities were reduced to acceptable levels. In this type of set-up the laboratory itself acts as an air plenum and little outside air is necessary for operation. Aside from the necessary air contraction and diffusion cones, the scheme accurately represents field installation conditions, which is not true of the closed loop circuit.

IV.1.3 OPEN CIRCUIT WITHOUT COOLING

The open circuit system, without air cooling, shown in Figure 24 not only duplicates the anticipated field installation conditions, with the exception of the contraction cone, but also requires the least space and expense during construction. The primary disadvantage of this

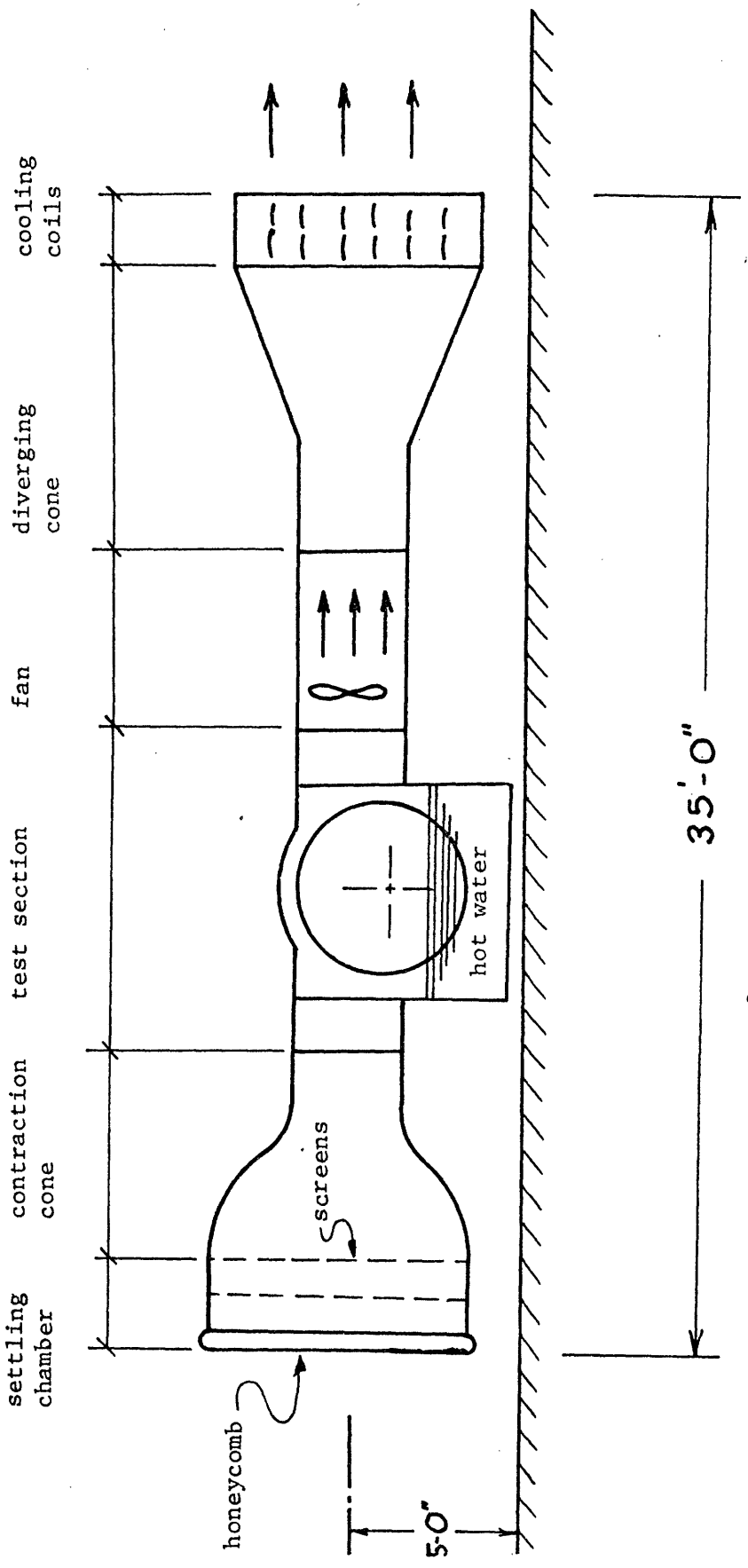

Open circuit loop with cooling

Figure 23

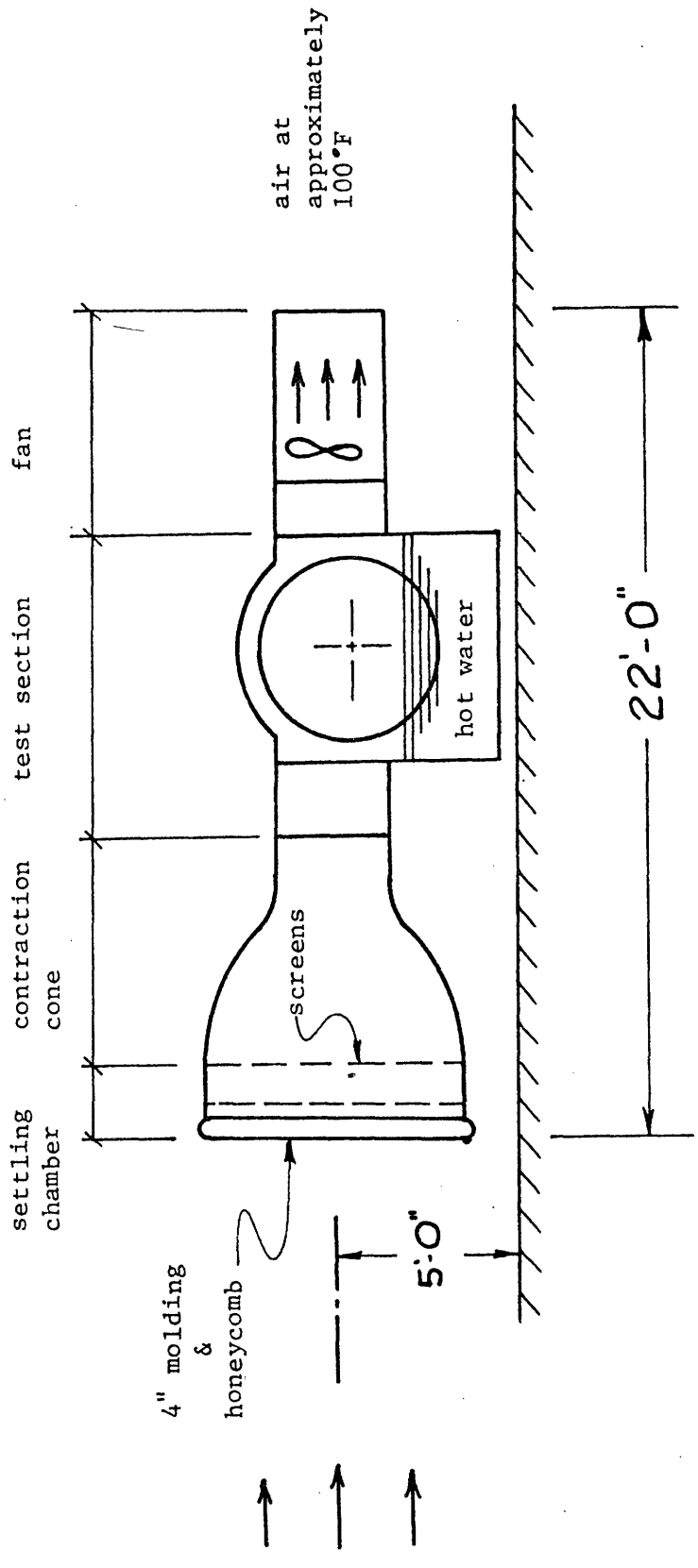

Open circuit loop without cooling

Figure 24

system is that it must either be constructed outside or in a very large room so that when operating at steady state conditions for an extended period of time the air temperature in the room will remain constant. In the actual design used, this problem is overcome by building the apparatus inside a large room and exhausting the warm air, at approximately 100°F, outside of the room. Make up or supply air is obtained from the atmosphere a sufficient distance away from the exhaust outlet so that no short circuiting effects are encountered in the atmosphere directly outside the room. The room itself is used as a plenum for this air.

The purpose for the honeycomb, screens, and contraction cone preceeding the test section in each of the three schemes is to provide for a uniform air velocity profile at the entrance to the test section. This will allow calculations to be made of the heat transfer characteristics of the exchanger by providing for accurate measurements of inlet air velocity, temperature, and pressure. The air streams entering the test section will also be parallel with each other, and by so being, will allow for experiments to be made to obtain an air baffle around the rotating discs that will establish a uniform pressure drop across them. Although the use of honeycombs, screens, and contraction cones is not anticipated in the actual field model, their use in the lab will allow overall exchanger performance to be optimized.

IV.1.4 COST ANALYSIS

Several cost analysis were made including the cost of installing the necessary utilities to the three proposed configurations in various different available locations at the Institute. The least expensive site was found to be offered by the Institute's Experimental Projects Laboratory (E.P.L.) using the open circuit system, with the hot air being exhausted to the atmosphere. A plan view of this location is shown in Figure 25 . This large room, with a 16 foot ceiling, provides a test area with all the required utilities, large open spaces between this experiment and other experiments in the room, and excellent air handling capabilities. Presently equipped with 2000 CFM room exhaust fan capacity, no sensible air currents are present when these fans were turned on in conjunction with the recently installed 5000 CFM air blower used in this experiment. The site is serviced with a 5 ton overhead crane and is located directly above the E.P.L. Laboratory shops.

A one foot wide test section of rotating discs was decided upon as being sufficiently wide to minimize end effects, such as heat loss through the test section's side walls, the resulting temperature gradients, and velocity profile irregularities caused by the stationary side walls, while being of such a size that construction expenditures were reasonable.

IV.1.5 UTILITY REQUIREMENTS

Calculations were made to determine the exact utility requirements for the test site of the full scale model of the periodic heat exchanger.

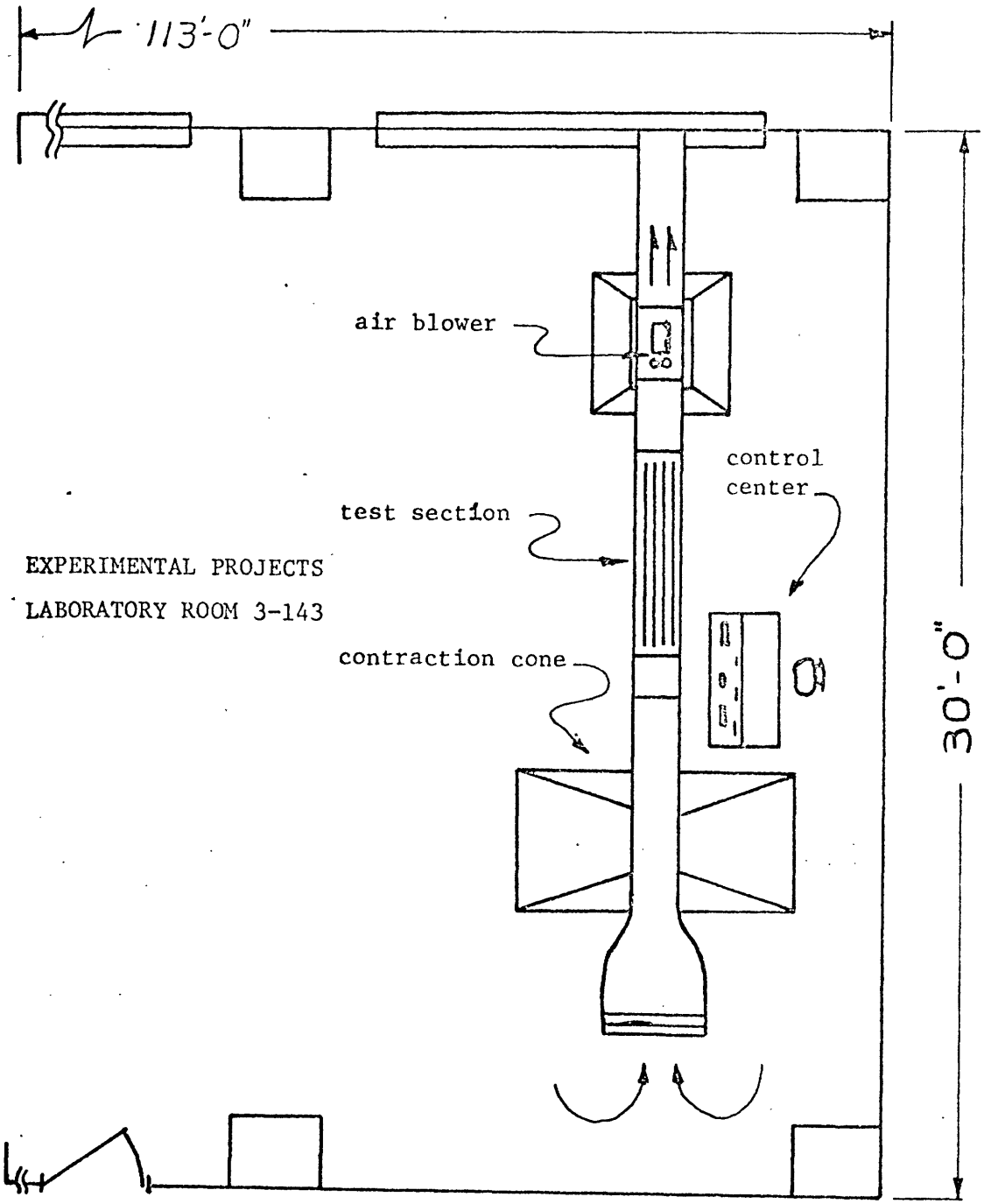

Site location - full scale model

Figure 25

These calculations were based on the results of a computer program which had optimized the major varables for a full scale, or five foot diameter, periodic heat exchanger. The results of these calculations are listed in Table 5.

Table 5

DESIGN CRITERIA FOR FULL SCALE MODEL OF

PERIODIC HEAT EXCHANGER WITH *SMOOTH DISCS

ITEM	DESCRIPTION PER HORTIZONTAL FOOT OF LENGTH
1. Thermal Capacity	0.045 MGW Thermal
2. Hot Water Flow Rate	32.4 gal./min.
3. Instanteous Hot Water Heater's Steam Flow	195 lbm./hr. @ 10 psig.
4. Area Contraction Ratio	9 to 1
5. Maximum Air Velocity	5200 CFM @ 2 in. water
6. Maximum Air Velocity	34.5 ft./sec.
7. Air Pressure Drop in Test Section	6.15 $lbf./ft.^2$
8. Disc Diameter	5 ft.
9. Disc Thickness	0.034 inches (22 B.W.G. gauge)
10. Disc Spacing	0.33 inches on centers
11. Disc Rotational Velocity	5-20 RPM
12. Disc Surface Finish	smooth (galvanized sheetmetal)

* The smooth discs referred to in this figure may possibly be modified later with roughness elements to increase the heat transfer. Different spacings would be required for these discs.

IV.2 OPEN CIRCUIT MODEL WITHOUT COOLING

IV.2.1 FLOW NONUNIFORMITIES AND LOW TURBULENCE

The upstream section of this model consists of an inlet, honeycomb, screens, and a contraction cone with the cones vertical dimension varable. Design of this section was influenced by three criteria; a uniform velocity profile and a low turbulence level was desired in the test section, and a varable vertical dimension was required in the test section to accomodate different diameter test discs.

IV.2.2 INLET

The inlet provides a direct opening to the honeycomb section. The cross section is 87 inches high and 36 inches wide. This inlet is located a minimum of five feet from the nearest wall to ensure smooth air entry into this section [8]. A one and one half foot clearance between the floor and the bottom of the inlet is provided. Design air entrance velocity to the inlet is 4 feet per second. To ensure a smooth entry of the air around the edges of the inlet, a 4 inch diameter moulding was attached to the perphery of the inlet.

IV.2.3 HONEYCOMB AND SCREENS

A honeycomb is utilized as a flow straightening device at the inlet. It aids in breaking up large scale eddies and swirls which maybe present

at the inlet, and also reduces the spread of tranverse air velocities [9]. The honeycomb is constructed of approximately 115,000 plastic soda straws, three sixteenth of an inch in diameter, and six and one half inches long, carefully stacked in a hexagonal close packed configuration and held in place fore and aft by #18 mesh aluminum screen. These plastic straws were made by an extrusion process which resulted in seamless construction and clean cut ends. Fine (#18 mesh) screens were installed in the settling chamber, upstream of the contraction cone, to reduce turbulence levels and to increase the uniformity of the velocity distribution (Figure 24). These screens remove large eddies and introduce a great number of small, higher velocity eddies which decay rapidly. The smoothing action of the screens is based on the fact that air static pressure losses are proportional to the square of the air velocity so that the relative velocity reduction of the faster moving air particles is much greater.

Gorlin [9] suggests that a velocity perturbation ΔV_1, upstream will produce a corresponding perturbation ΔV_2 downstream where

$$\Delta V_2 = \left(\frac{2-\zeta}{2+\zeta}\right) \Delta V_1 \tag{11}$$

Here ζ is the resistance coefficient of the screen defined as

$$\zeta = \left(1-\bar{f}\right) + \left(\frac{1-\bar{f}}{\bar{f}}\right)^2 ; \quad \bar{f} = \frac{F_1 - F_3}{F_1} = \frac{F_3}{F_1} \tag{12}$$

where F_3 denotes the projected area of the screen wires and F_1 the frontal area of the cross section. To minimize the turbulence caused by the screen itself, it is necessary to use a net made from wire of very light gauge and install it in the settling chamber, the section of minimum velocity and hence where losses from screen installation are

a minimum. The Reynolds number for #18 gauge mesh at the design air velocity is 32. It is reported [8] that if this number is below 40 the turbulence arising from the screen will be so slight that it will decay completely upstream of the test section. Each screen installed in the settling chamber was cut from a three foot continuous roll to avoid seam imperfections. Each screen, as well as the honeycomb section, is mounted on a readily removable frame in case the need for a replacement should arise.

The difference commonly observed between tests made in different wind tunnels at the same Reynolds number and the results observed in atmospheric condidtions indicate that some correction is needed to account for the effect of the turbulence present in the air entering the wind tunnel and more importantly, the turbulence created in the wind tunnel by vibration and imperfections in the tunnel walls. It is shown [10] that this turbulence will cause the flow pattern in the tunnel to be similar to the flow pattern in free air at a higher Reynolds number. Therefore the tunnel test Reynolds number could be said to have a higher effective Reynolds number. This increased ratio is called the turbulence factor and is defined by

$$Re_e = TF \times Re \tag{13}$$

This correction factor will be applied to the raw data obtained in this experiment to ensure that the proper heat transfer coefficients are obtained.

Turbulence may be measured with a turbulence sphere[10], which is a smooth sphere, of varying diameter, having an orifice at the front stagnation point and four more interconnected and equally spaced orifices in the back of the sphere, $22\frac{1}{2}$ degrees from the axial line of the sphere.

A drag coefficient C_d is then defined[11] as

$$\text{Drag} = (C_d)(A)\frac{\rho U^2}{2} \tag{14}$$

in which A is the projected area of the body on a plane normal to the flow.

The drag coefficient of a sphere is affected greatly by changes in air velocity[10]. Contrary to the layman's guess, C_d for a sphere initially decreases with increasing air speed since the results of an earlier transition of the air boundary layer to turbulent flow is that the flow adheres to the surface of the sphere for a longer period of time. This is because the high momentum transfer in the turbulent boundary layer delays flow separation from the sphere so that it's wake is substantially reduced. This action decreases the form or pressure drag, resulting in a lower total drag coefficient. The decrease is so rapid in one range that both the drag coefficient and the drag go down. Obviously, the Reynolds number at which the transition occurs at a given point on the sphere is a function of the turbulence already present in the air, and hence the drag coefficient of a sphere can be used to measure turbulence. One method is to measure the drag for a small sphere 5 or 6 inches in diameter, at many tunnel speeds. After

subtracting the test specimens shape factor, or bouyance (equation 10), we may compute the drag coefficient from equation 3. The sphere drag coefficient is then plotted against the calculated Reynolds number, Re (Figure 26), and the Reynolds number at which the drag coefficient equals 0.30 is noted and termed the critical Reynolds number, Re_c. The above particular value of the drag coefficient occurs in free air at a Reynolds number equal to 385,000, so it follows that the turbulence factor TF, is

$$TF = 385{,}000/Re_c \qquad (15)$$

The effective Reynolds number, Re_e, may then be found from equation 13. A second method, and the one to be used in this experiment, of measuring the turbulence in a wind tunnel makes use of a pressure sphere [10]. No force tests are necessary with this method and the difficulties of finding the support drag in the tunnel are eliminated. The pressure sphere has an orifice at the front stagnation point and four more interconnected and equally spaced orifices at $22\frac{1}{2}$ degrees from the theoretical rear stagnation point. A pressure lead from the front orifice is connected across a manometer to the lead from the four rear orifices. After the pressure difference due to the static logitudinal pressure gradient caused by the test specimen in the test section is subtracted, the resultant pressure difference, ΔP, for each Reynolds number is divided by the dynamic pressure for the appropriate Re, and the quotient is plotted against Re (Figure 27). It has been found that the pressure difference $\Delta P/q$ is 1.22 when the sphere drag coefficient C_d is 0.30,

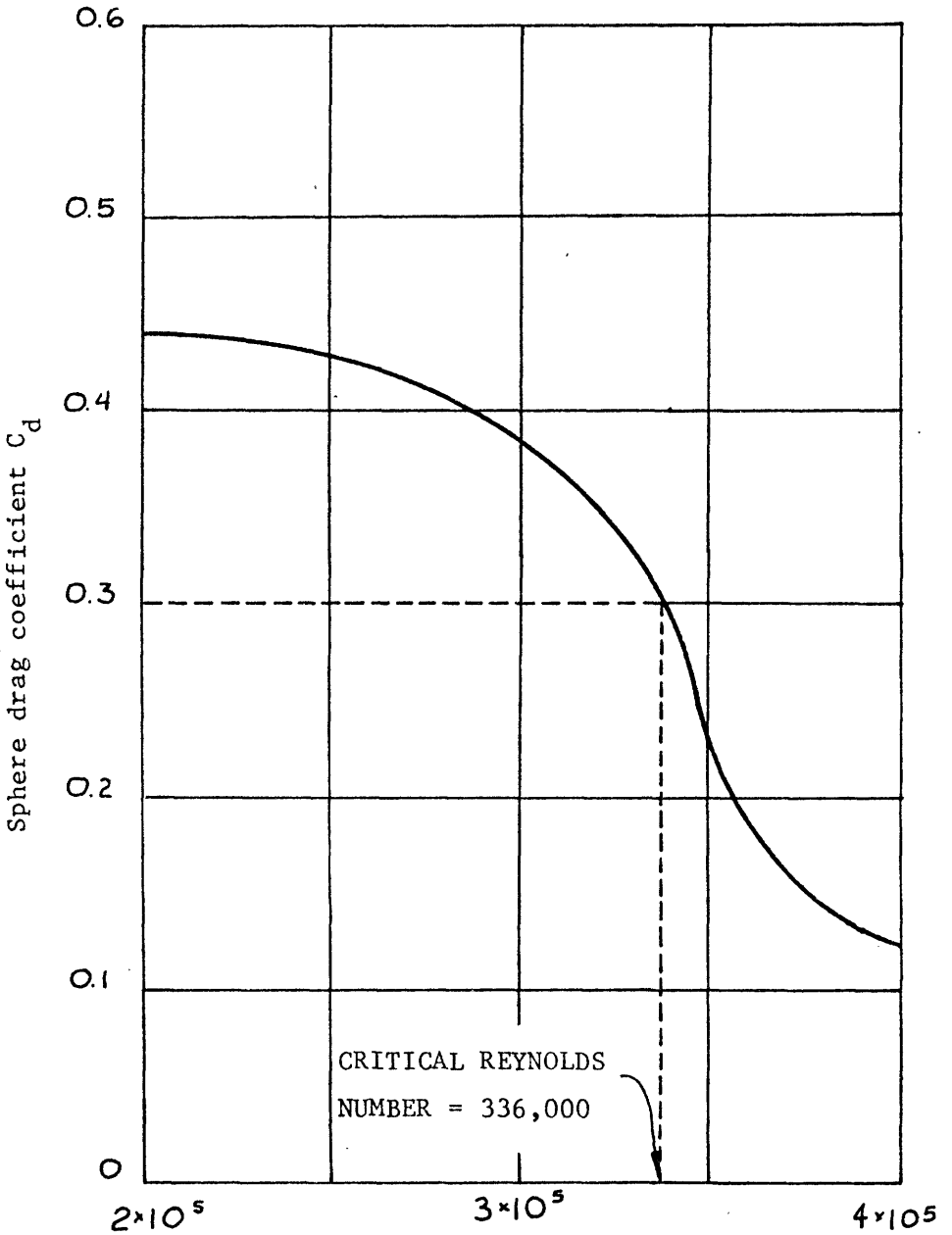

Plot of C_d vs. Re

Figure 26

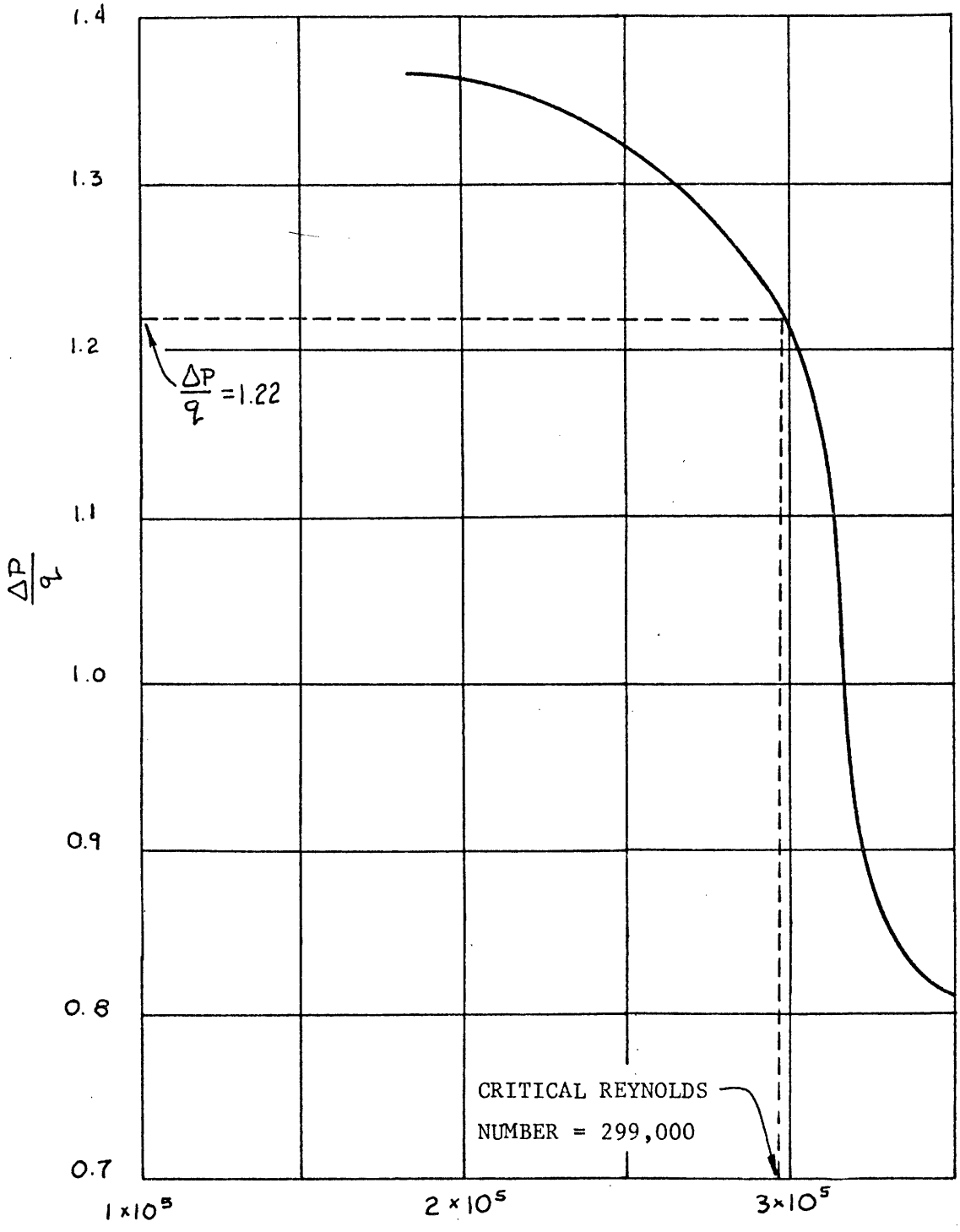

Plot of $\frac{\Delta P}{q}$ vs. Reynolds number

Figure 27

and hence this value of $\Delta P/q$ determines the critical Reynolds number. The turbulence factor may then be determined as before.

Turbulence factors vary from 1.0 to about 3.0 [10]. A value of 1.7 is normally expected in a student tunnel. Although it appears from the above discussion on turbulence that high turbulence yields high effective Reynolds numbers, it has been shown [10] that the above corrections are not exact and that excessive turbulence makes test data difficult to interpret. Turbulence levels may be lowered to acceptable levels in a given wind tunnel by the simple addition of screens, usually in the settling chamber. These damping screens will reduce the intensity of turbulence according to the relation

$$\frac{U_3'}{U_1'} = \frac{1}{(1+K)^{n/2}} \qquad (16)$$

where 1 and 3 refer to stations ahead of and behind the damping screens, U is the root mean square of the velocity fluctuations in the three principal Cartesian coordinate directions and is referred to as the percent of turbulence (Figure 28), n is the number of screens, and K is the pressure drop through one screen in units of dynamic pressure (Figure 29). In this experiment K is equal to 1.3 and since three screens are used, the ratio of U_3/U_1 predicted is 0.29.

It should be noted that station 3 must be sufficiently far down stream (several feet) so that the turbulence caused by the screens themselves has time to dampen out. The spacing between screens seems to make no difference as long as they do not touch [12].

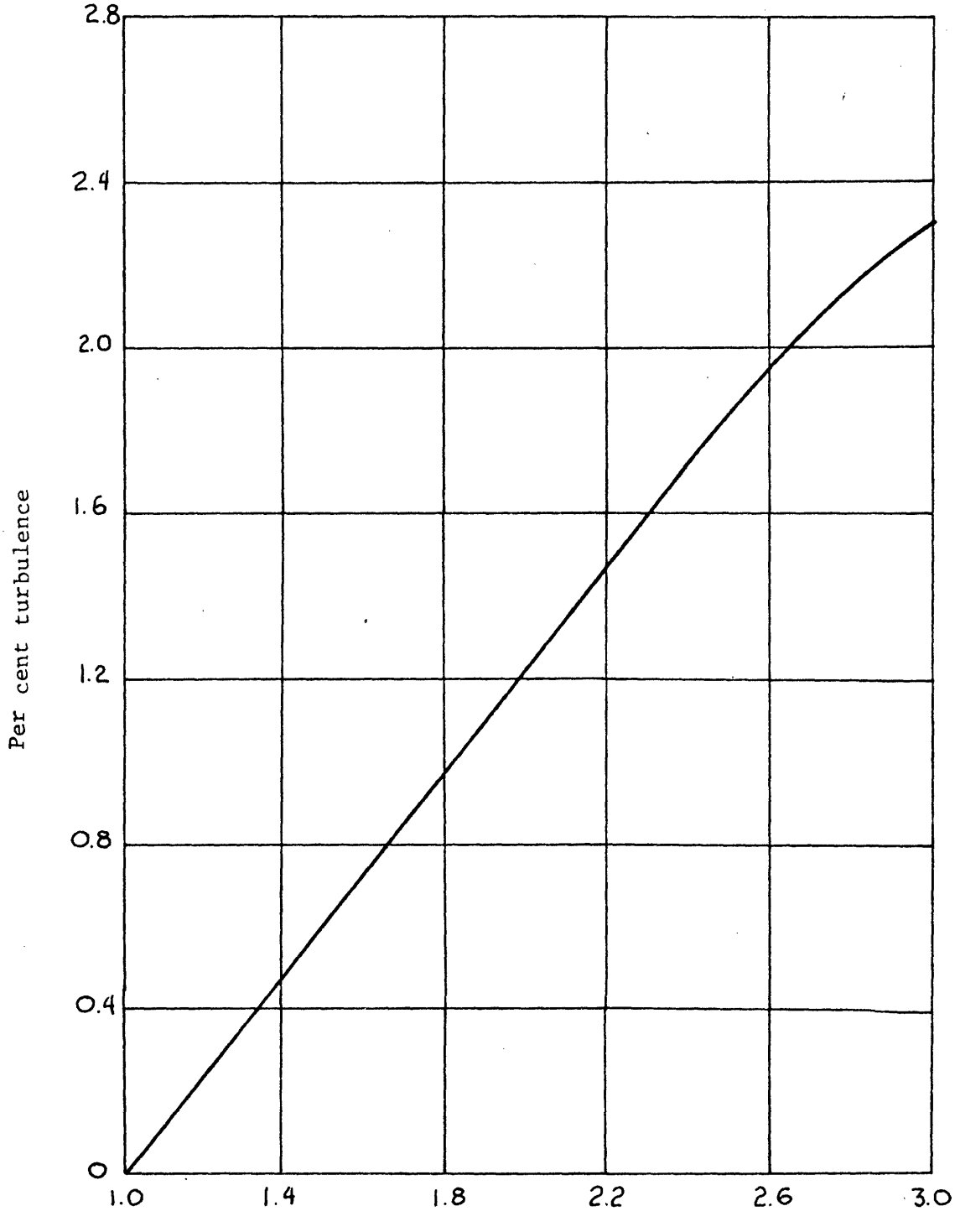

Plot of % turbulence vs. turbulence factor

Figure 28

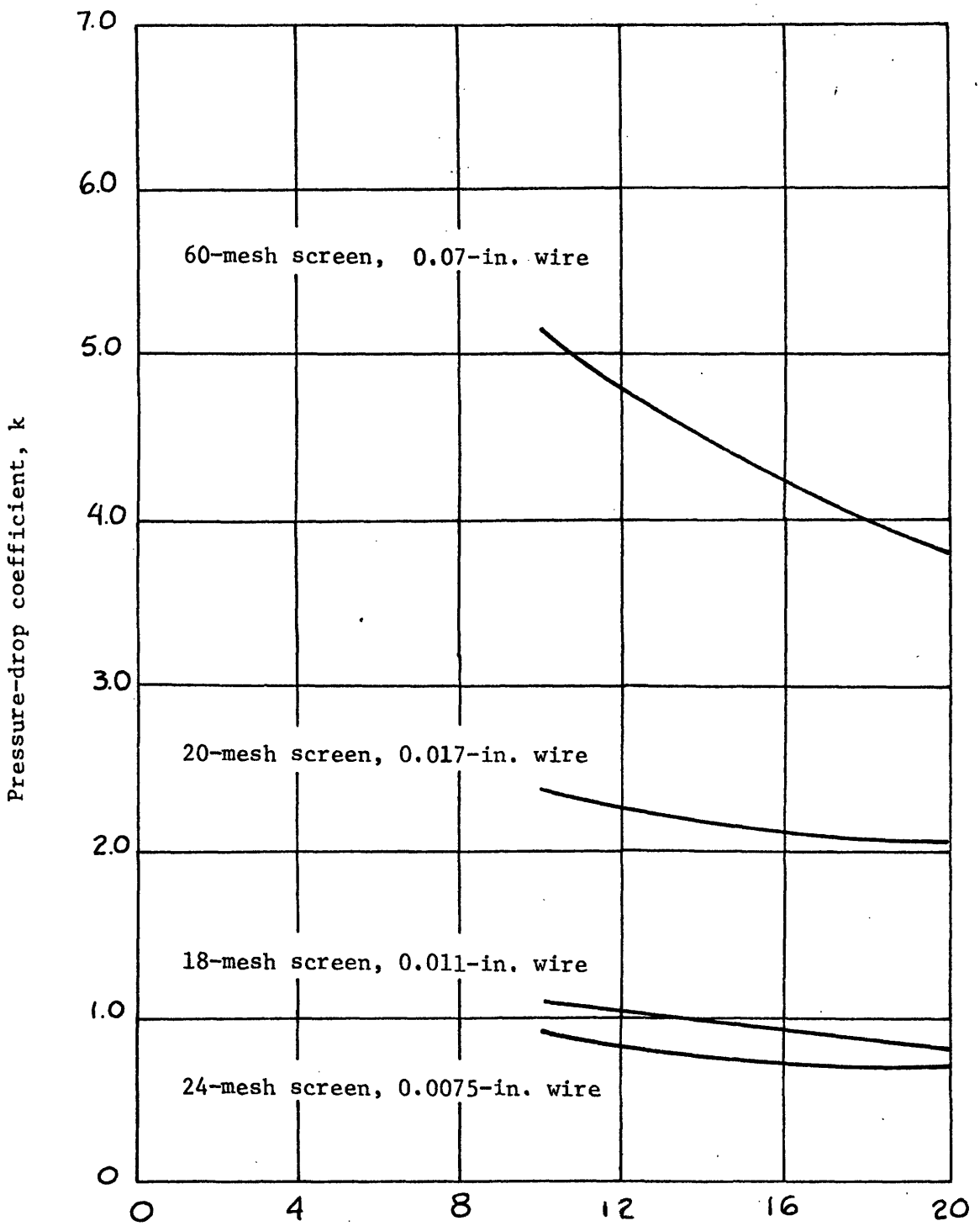

Plot of k vs. velocity in settling chamber - Figure 29

Excessive screens, while resulting in very low turbulence levels, increase the fan power required in the tunnel and should be avoided. A turbulence factor of less than 1.4 will be obtained in this experiment.

IV.2.4 CONTRACTION CONE

The principal function of the contraction cone is to accelerate the low-speed air entering it from the settling chamber to the velocity required in the test section. In addition, because of its gradually decreasing cross section, the contraction cone reduces the velocity nonuniformity. The shape and dimensions of the contraction cone determine not only the magnitude of the velocity, but also its uniformity, and affects the evergy losses in the cone due to the air friction at the walls. The velocity variations in the test section maybe calculated from the velocity variations in the settling chamber. It can be shown [9] that

$$\frac{\Delta V_1}{V_1} = \frac{n^2 \, \Delta V_2}{V_2} \quad \text{(Figure 30)} \qquad (17)$$

where V is the velocity at the point indicated, ΔV is the varation in velocity across the cross section, and n equals the contraction area ratio. Thus the velocity variations in the test section are n^2 times less than the velocity variations at the nozzle inlet.

The contraction ratio was limited by the space available at the test site and construction costs. An area ratio of 9 to 1 was decided upon, with a one foot by two foot six inch test section. This was felt to be adequate to test the performance of a five foot diameter full

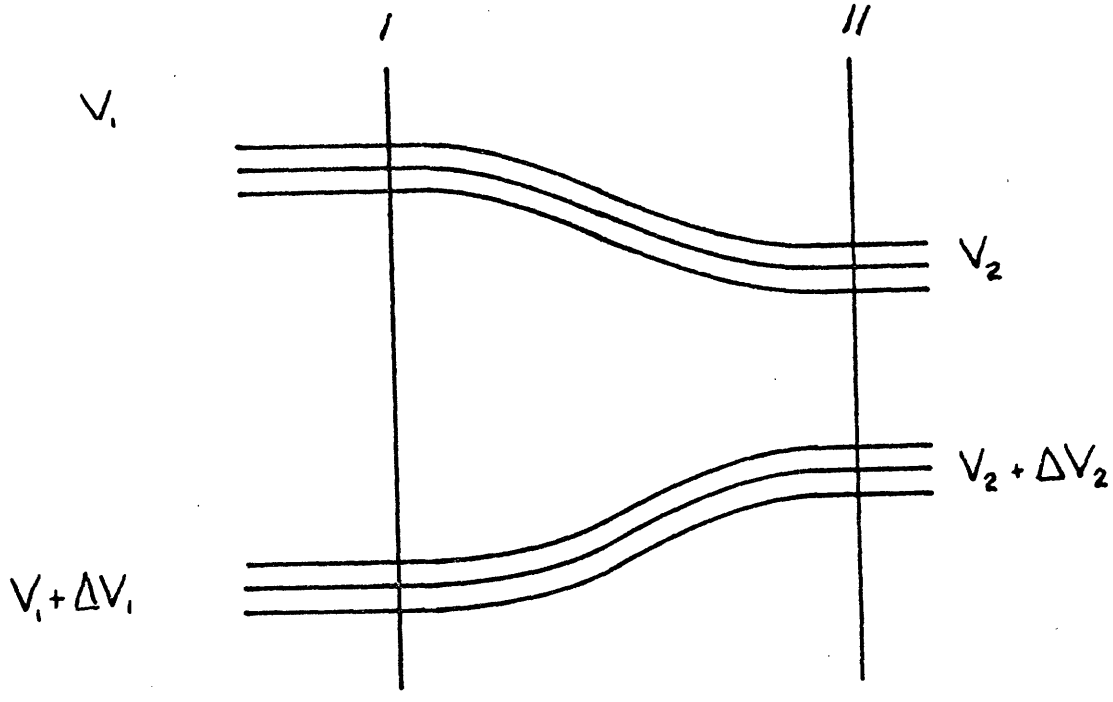

Velocity equalization in a contraction cone

Figure 30

scale periodic exchanger disc. The vertical height was made varable so that different diameter test discs could be tested with only minor changes to the test apparatus.

It should be noted that the use of honeycombs, screens, and contraction cones permit the test specimens to be evaluated under ideal, low turbulence, uniform velocity conditions. Any flow nonuniformities thru the discs will consequently have been created by the discs themselves rather than by the inlet. Any flow abnormalities caused by the inlet will, of course, increase the turbulence levels in the test section. This increase will result in a more rapid boundary layer transition from laminar to turbulent and increase the heat transfer coefficients calculated from the data. Therefore, the lower the turbulence levels obtained, the more conservative the test results.

IV.2.5 CONTRACTION CONE THEORY

There are many methods in use to determine the actual shape of a contraction cone. The principle criteria is that the given shape does not allow separation to occur along the walls as this could cause extreme fluctuations at the test section. Theoretical approaches have been limited to potential flow considerations, and are not directly applicable to this case.

Tsien [13] has developed a ninth degree polynomial curve for a contraction cone profile. This curve is based on the fact that if the velocity at the tunnel wall is made to increase monotonically from the beginning of the cone to the end, the pressure along the wall will always be decreasing and the danger of boundary layer separation is avoided.

Maestrello [14] has reported having success with a contraction cone which follows Tsien's curve. This curve is shown in Figure 31 and was obtained by setting the first three derivatives in the equation to zero at the inlet to ensure a smooth entrance into the cone, and setting the first five derivatives to zero at the exit to ensure the exit from the cone is smooth.

Hansen [8] has determined through scale model testing that the problem area of such a design is at the exit of the cone and concentrated his work on this region. Accordingly, he has improved on Maestrello's design by setting the first two derivatives to zero at the inlet and setting the first six derivatives to zero at the exit to ensure a smoother flow in this region (Figure 32). It can be seen that Hansen's curve provides a more gradual velocity change at the wall in the exit region. Since a more gradual velocity change decreases the possibility of boundary layer separation, Hansen's modified equation was selected.

Two ninth degree polynomial curves were drawn which gave the desired 9 to 1 contraction ratio by specifying the correct coefficients for Hansen's modified equation. These along with the contraction ratio serve to specify each of the ten constants for the derivatives resulting in the following equations

$$y = 11.50\,\frac{\xi^7}{6^7}\left(\frac{7}{9}\xi^2 - \frac{21}{2}\xi + 36\right) \quad \text{where} \quad \xi = \frac{x}{12} \tag{18}$$

$$y = 28.75\,\frac{\xi^7}{6^7}\left(\frac{7}{9}\xi^2 - \frac{21}{2}\xi + 36\right) \quad \text{where} \quad \xi = \frac{x}{12} \tag{19}$$

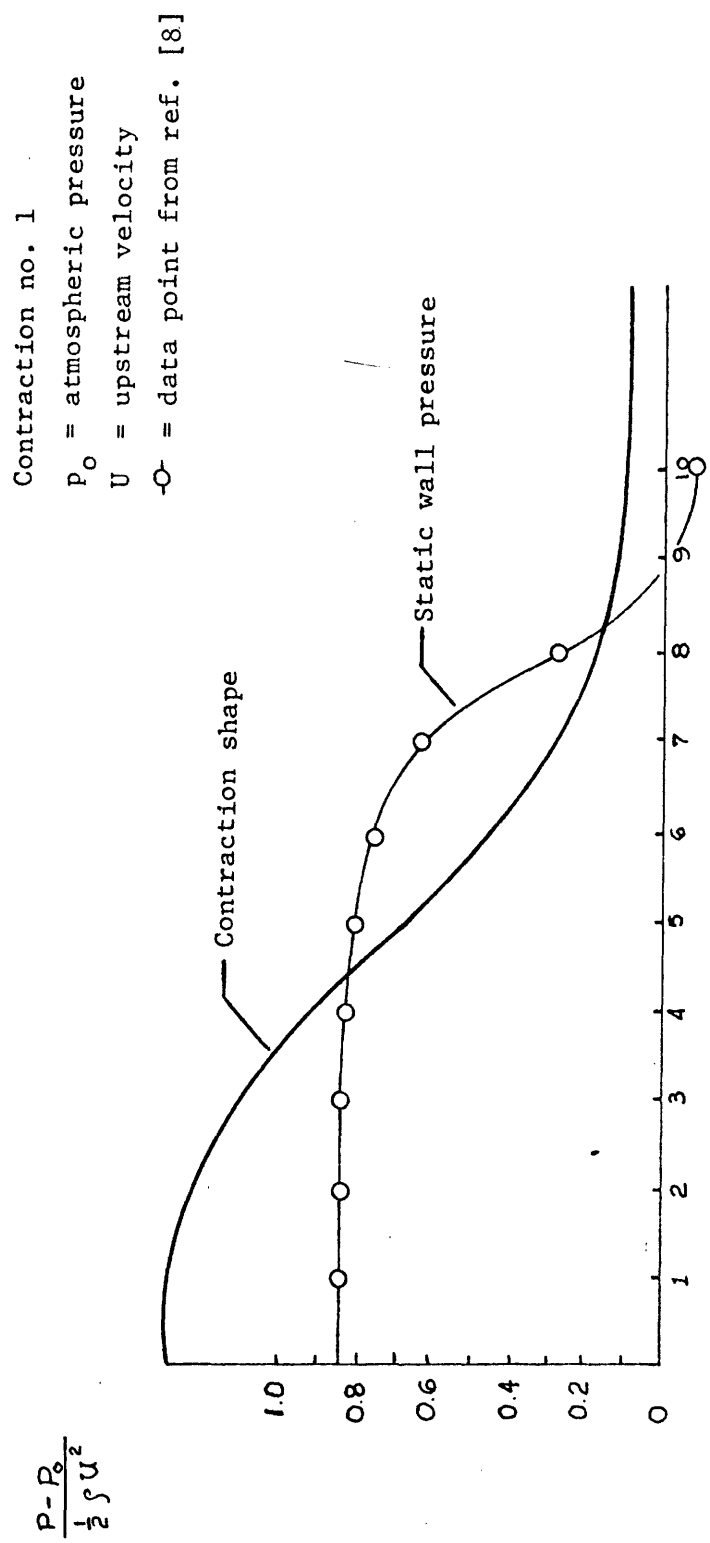

Static pressure distribution along model contraction section wall

Figure 31

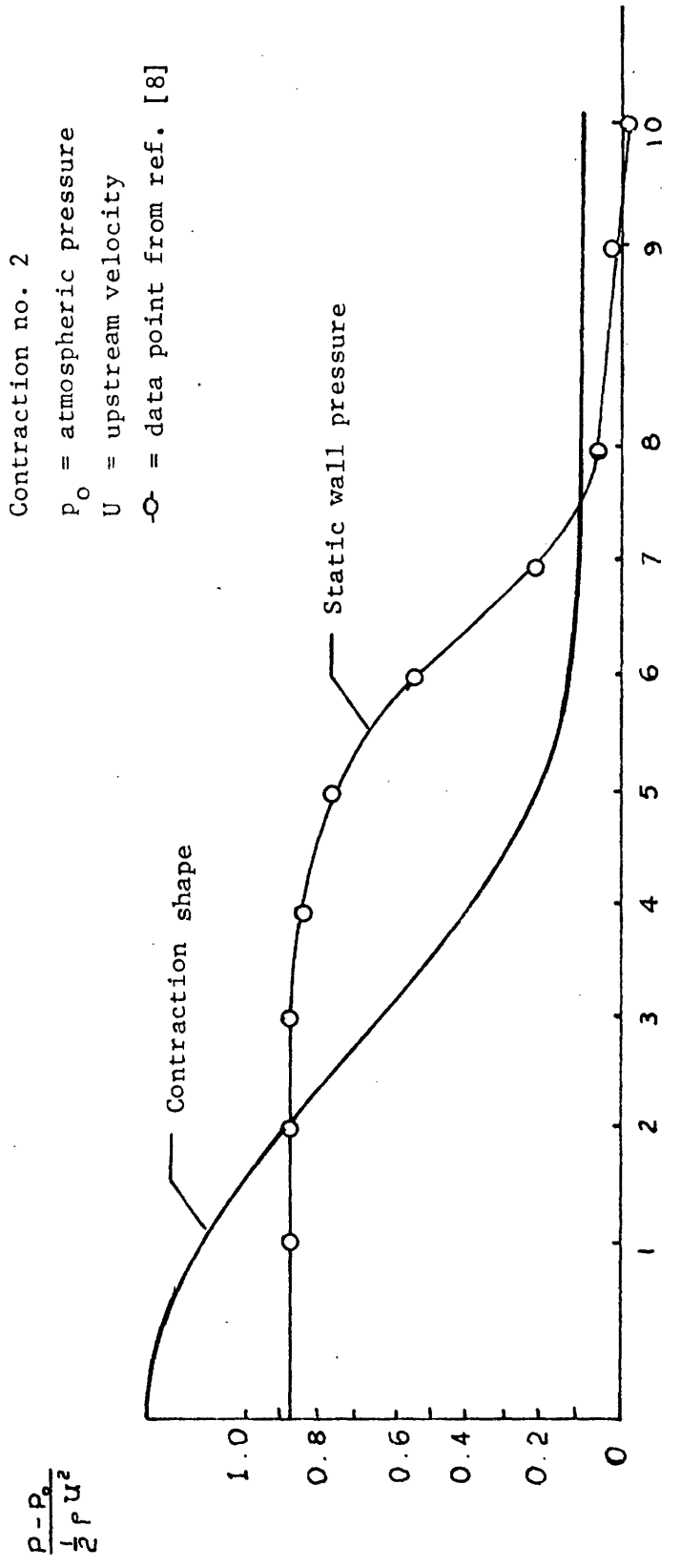

Static pressure distribution along model contraction section wall

Figure 32

These curves have the shape shown in Figure 33 and Figure 34 , and provide the desired reduction in area along the centerline of the contraction cone.

Due to the difficulty in fabricating a compound curve in three dimensional space, it was decided to fabricate the contraction cone in two steps. In the first step of three feet, the vertical dimension was fixed while the hortizontal dimension was allowed to follow the desired curve (Figure 35). In the second step, the hortizontal dimension remained essentially fixed, although it did vary approximately one inch in six feet as specified by the last portion of Figure 36 ., while the vertical dimension followed the desired curve (Figure 35). This greatly simplified construction, and is recommended by Gorlin [9] where construction capabilities are marginal. The contraction cone is constructed from wooden sides reinforced with steel angle and overlayed with one eighth inch masonite for the tunnel surface.

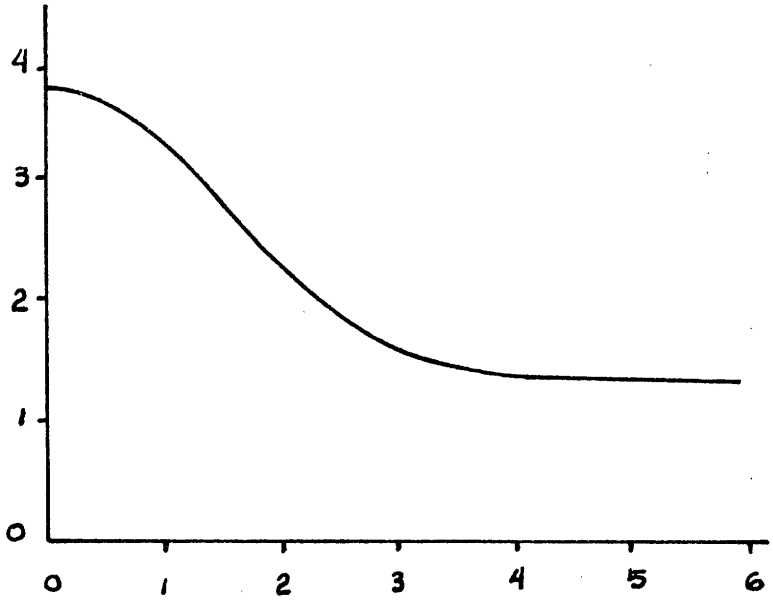

Wall section of contraction cone - vertical cross section

Figure 33

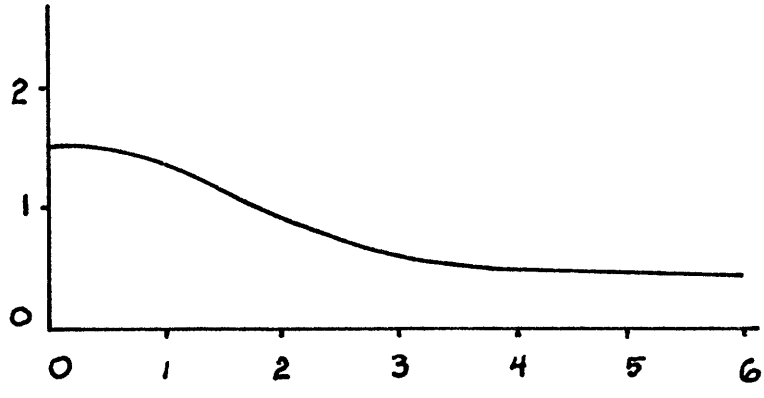

Wall section of contraction cone - hortizontal cross section

Figure 34

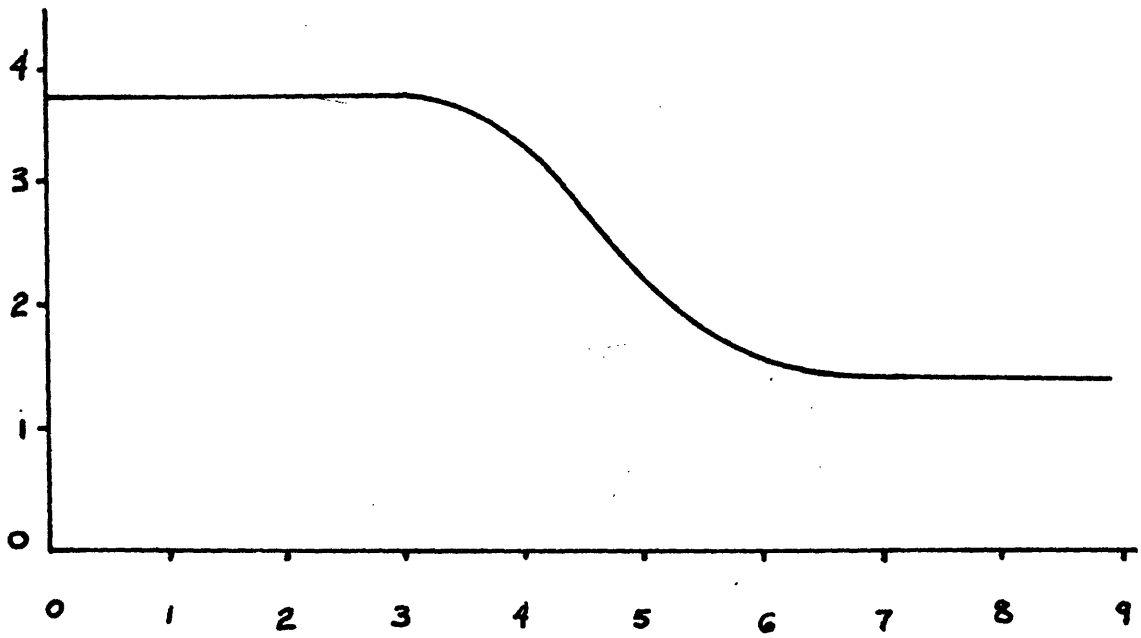

Wall section of contraction cone - vertical cross section

Figure 35

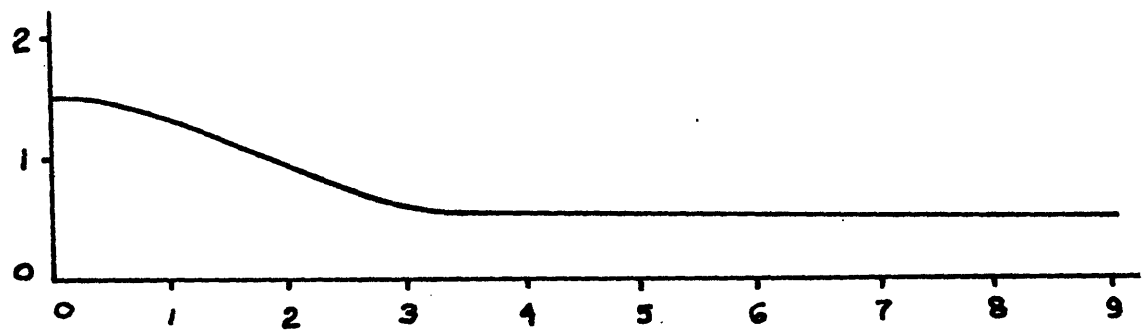

Wall section of contraction cone - hortizontal cross section

Figure 36

IV.3 INSTRUMENTATION

IV.3.1 CONTRACTION SECTION

The free stream velocity will be measured by the static-pressure drop between the two sections of the tunnel. These static pressure taps are located in the settling chamber and the entrance to the test section, far enough away from the model to be unaffected by its presence. The total pressure difference between these two sections will be equal to the losses between them

$$P_1 + \frac{\rho V_1^2}{2} = P_2 + \frac{\rho V_2^2}{2} + K_L \frac{\rho V_2^2}{2} \qquad (20)$$

where K_1 is the loss coefficient [9], determined from a given calibration curve for the tunnel

$$K_L = \frac{\Delta P_{measured} - \Delta P_{true\ STATIC\ PRESSURE}}{\Delta P_{true\ STATIC\ pressure}} \qquad (21)$$

and P_1, P_2, V_1, V_2, are the static pressures and velocities in section 1 and 2 respectively (Figure 30). If the cross section at 1 and 2 and the area of the test section at 3, where the test discs are located, are F_1, F_2, and F_3 respectively, then according to the continuity equation for an incompressible fluid

$$F_1V_1 = F_2V_2 = F_3V_3 \qquad (22)$$

Substituting the values of the velocity heads in sections 1 and 2, expressed through the velocity head in the test section 3, into equation 20, we obtain

$$P_1 - P_2 = Z \frac{\rho V_3^2}{2} \tag{23}$$

where

$$Z = \left(\frac{F_3}{F_2}\right)\left[1 + K_L - \left(\frac{F_2}{F_1}\right)^2\right] \tag{24}$$

Using this equation we can obtain the velocity head in the test section of the tunnel, by measuring the static pressure drop between sections 1 and 2. For this purpose we must know Z. This is determined by calibrating the empty tunnel with a pitot-static tube. At different flow velocities the average value of the velocity head in section 3 is determined simultaneously with the pressure drop $P_1 - P_2$. The value of Z can be found from these measurements. From equation 23

$$V_3 = \left(\frac{2(P_1 - P_2)}{\rho Z}\right)^{\frac{1}{2}} \tag{25}$$

Surveys across areas A_1 and A_2 will be taken with a pitot-static tube to be assured that actual velocities do not vary significantly from the mean values. For a more accurate measurement of the pressure drop between sections 1 and 2 of the contraction cone, duplicate static pressure taps, interconnected with tubing, have been installed.

IV.3.2 TEST SECTION

The test section will consist of the rotating discs, a hot water bath, and a varable air baffle which will be adjusted for different periodic disc diameters. This unit will rest on heavy semi-steel casters and will be movable for better access to the supporting equipment. A one half inch thick plexiglass window in this section will allow oil, water, and air circulation to be viewed from the outside during operation. A varable speed D.C. motor and voltage control will provide for the varable speed rotation velocities of the periodic discs. A hot water system has been constructed which will provide a continuous supply of 140°F hot water to the test section (Figure 37). Two hundred pound steam is used to supply heat to this system. Its pressure is reduced to approximately 5 to 10 psig. in a two stage pressure regulator before it enters the heat exchanger. The amount of steam entering the exchanger is controlled by a temperature sensor in the discharge line which monitors the exit temperature of the hot water and allows more steam to enter when the temperature of the water in this line falls below a predetermined temperature. Final control is obtained by using a one inch temperature control mixing valve, similar to those used in motion picture film processing units. This unit will allow a certain percentage of the water flowing thru the system to by-pass the heat exchanger and is designed to obtain temperature control within one degree Farenheit. A 2 H.P. 3600 RPM centrifugal pump is used to circulate the water through the system.

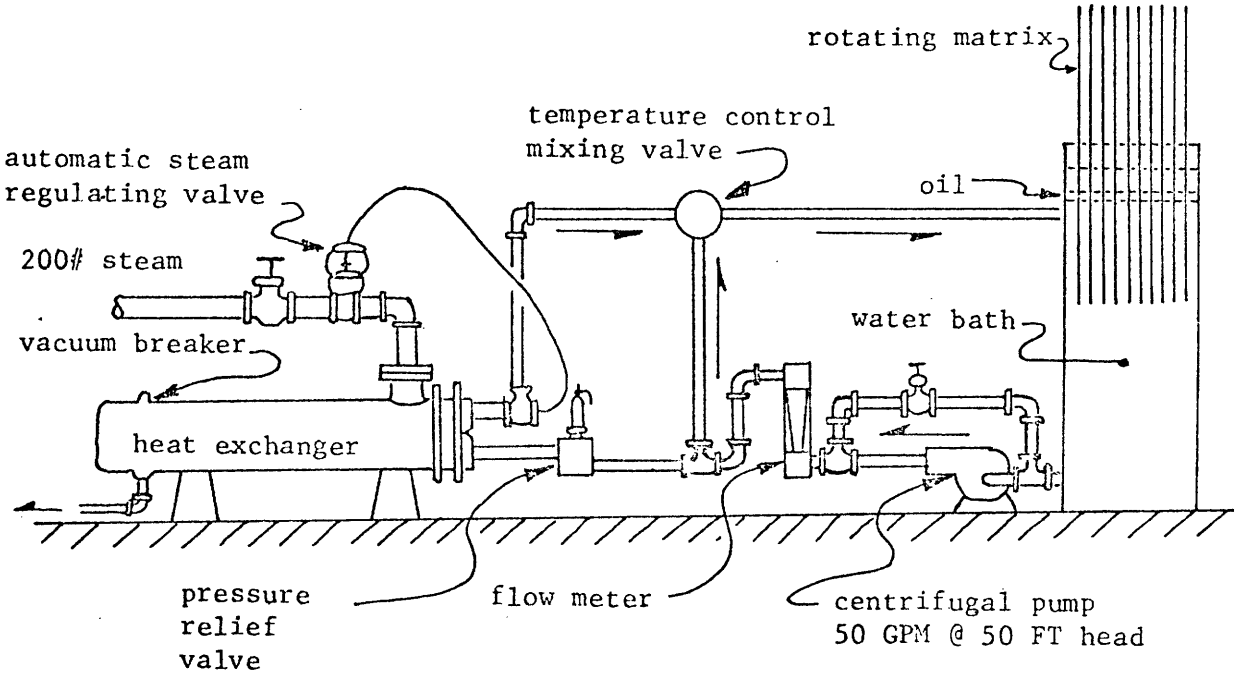

Hot water system - elevation view

Figure 37

a by-pass loop is provided around this pump to vary the pump's capacity to the desired flow rate, which is measured with a standard glass roto-meter. A pressure relief valve is installed in the system to protect against excessive pressures should a line become blocked or fouled during operation.

IV.3.3 AIR BLOWER

The air blower is a Buffalo vaneaxial type fan. The blower wheel has four propeller type blades and is driven by two enclosed rubber V-belts on a varable diameter sheave. The fan belt is powered from a 208 volt 3 phase electric motor mounted outside the airstream and rated at 5 H.P. @ 3600 RPM. This arrangement allows the capacity of the blower to be varied over the desired range of air flow.

IV.3.4 AIR SURGES

Air surges of up to 5 percent of the total tunnel flow may be caused by either of two separate phenomenon [15]. Surging may be associated with the separation and reattachment of the boundary layer within the tunnel, or it maybe caused when the experiments' air system characteristic air curve intersects the fan curve at two or more points. Boundary layer separation is usually associated with a diverging portion of an air system, of which there are none in this system, and since Hansen's modified contraction curve is being used in the converging portion of this system, this problem is not anticipated. If the operating point of the air system intersects the characteristic air curve of the fan in two or more places, the resulting instability

may cause surging. This may be eliminated by either adding or subtracting system resistance until a stable condition is reached. For this reason, a varable opening is provided for air flow between the test section and the fan. The opening or closing of this air gap will reduce the systems air resistance and eliminate any instability in the system. The exhaust air is blown out of the building through a sheetmetal duct and louver system and through an 18 x 32 inch opening thru the wall at an elevation of fifteen feet above the ground.

IV.4 TEST PROGRAMS FOR THE FULL SCALE MODEL

Test programs will be run for determing the overall air side and water side heat transfer coefficients, optimum disc rotational speed, disc surface stiffeners, and air and water distribution characteristics.

IV.4.1 AIR AND WATER HEAT TRANSFER COEFFICIENTS

Calibration curves will be made for the air contraction cone. The basic calibration curve for this purpose should be obtained from a pitot tube traverse across the test section. An effective Reynolds number (Equation 13) for the air flow between the discs could then be obtained using a pressure sphere as described on page 69 of this report to account for any turbulence that exists in the test section. The air flow rate through the test section may then be obtained from one manometer reading the difference between the static air pressure at the inlet and the outlet of the contraction cone. A manometer which operates through a bellows and a magnetic couple connected to the indicating pointer has been obtained for this purpose. Two percent accuracy is anticipated for this instrument. Room air temperature measurements will be obtained from a standard mercury thermometer. The temperature of the exit stream will be obtained from a thermocouple survey made across the test section.

The water flow rate through the water bath will be obtained from a roto-meter flowmeter, which simply measures the total flow across the discs in the bath. Water temperature will be measured with bimetalic thermometers fore and aft of the test section.

Having obtained flow rates and temperature changes of both the air and the water, an energy balance should be made to check the accuracy of the measurements. Overall heat transfer coefficients may then be obtained, following the procedures outlined by Robertson [1].

IV.4.2 ROTATIONAL SPEED

The optimum rotational speed for the discs should be obtained. This speed will best be found experimentally by rotating the discs at a fixed air velocity until the oil-water interface becomes mixed. When this occures, the oil will be displaced from its stationary position between the air and water and will enter the water loop. This will be considered to be an undesirable condition for the system and the rotational speed should then be reduced slightly. Since a D.C. motor will be used to spin the discs, power requirements for this operation may be determined by simply measuring the current and voltage supplied to this motor. A series of such test results plotted against air velocity will provide sufficient information for disc rotational speed optimization in conjunction with the entire heat exchanger.

IV.4.3 STRUCTURAL SURFACE RIBS

Since the cost of a periodic heat exchanger will be directly proportional to the surface area of the discs, it is desirable to spin

the discs as fast as possible, thus allowing the discs to be very thin and thereby reducing the overall costs of the system. However, discs of this nature are susceptable to vibration and buckling when wind loads are applied. For example, should the discs be placed by accident at a slight angle to the air flow, they would be subject to an accordingly slight wind load. A sample five foot disc of 22 B.W.G. gauge sheetmetal has been obtained and it is obvious from observation of this model that stiffening is required. Radial or circumferential ribs should be stamped in these discs to increase the average section modulus of the discs until they become structurally independent. These test discs should then be placed in the test section and tested at various angles of offset until satisfactory results are obtained. It should be noted that approximately the lower one third of the discs will be in the hot water bath. The water should act as a damper to high energy, high frequency vibrations of the discs.

IV.4.4 AIR AND WATER BAFFLES

Having arrived at an optimum disc rotational speed, different shaped air and water baffles should be used to obtain geometries that provide a uniform pressure drop across the discs. These baffles would be circular in shape and be located on the top (air side) and bottom (water side) of the rotating discs with a minimum of clearance between the discs and the baffles. Their primary purpose is to eliminate significant quantities of air and water from passing across the discs without being cooled or heated by them. Smoke streams should provide

adequate visual means of adjusting the air baffles, while dye markings could be used on the water side.

IV.5 PROGRESS COMPLETED TO DATE

The following figures show the progress that has been made to date on the construction of the full scale model of the periodic heat exchanger. Schematic diagrams of the various systems follow.

Steam schematic

Figure 44

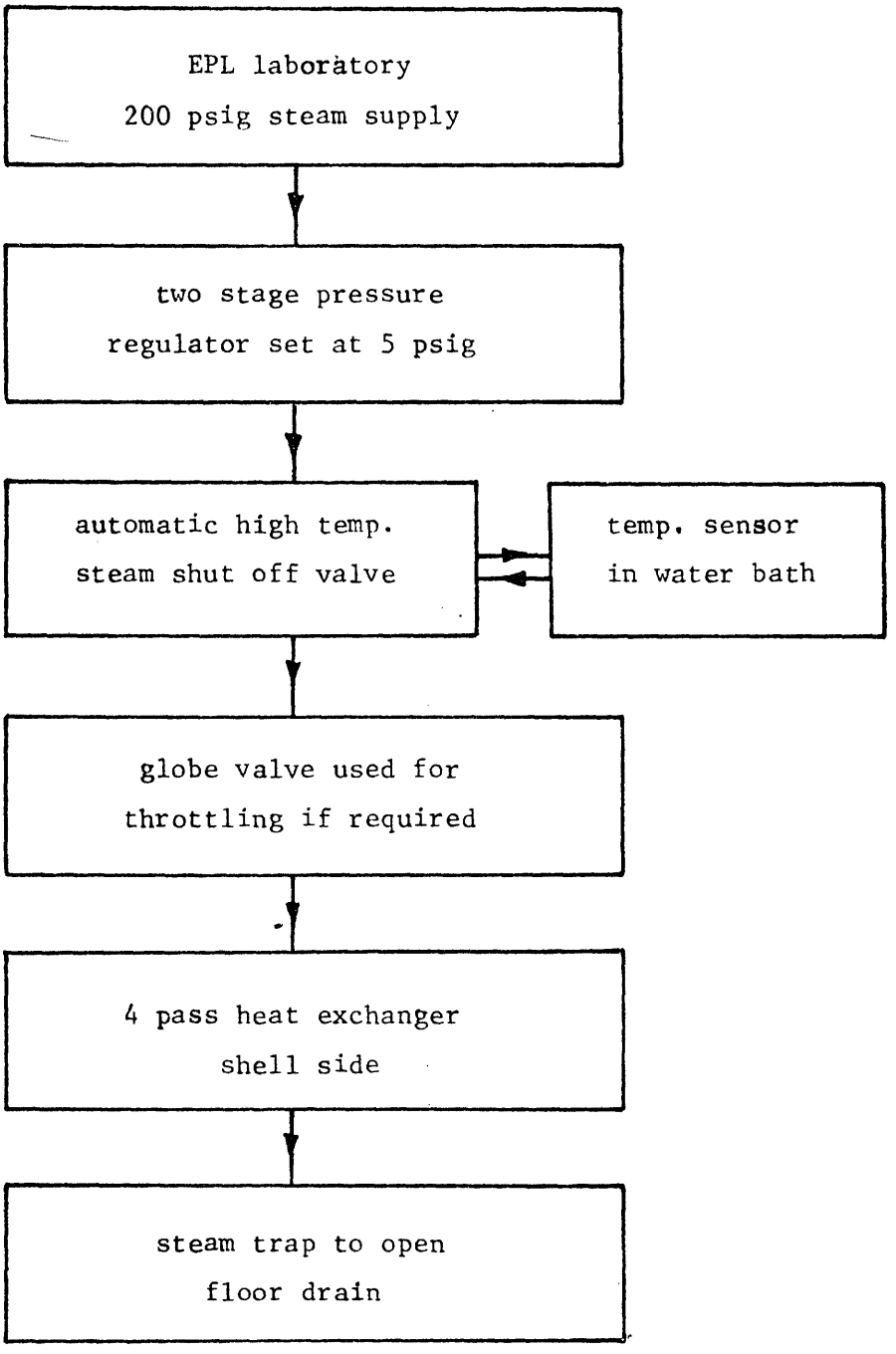

Hot water system schematic

Figure 45

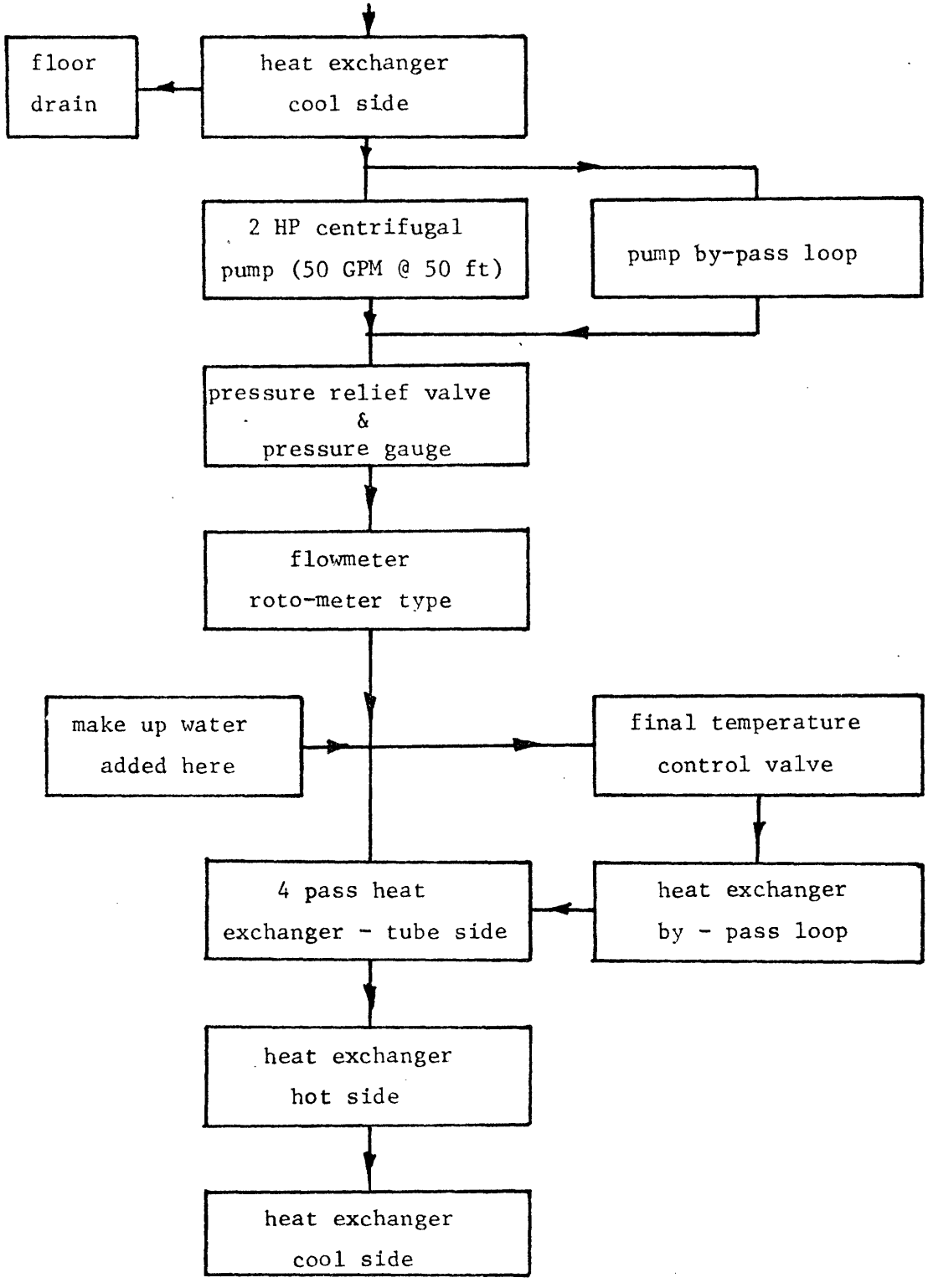

Figure 46

Electrical schematic for 5 HP air blower rated 5000 CFM at 2 in water

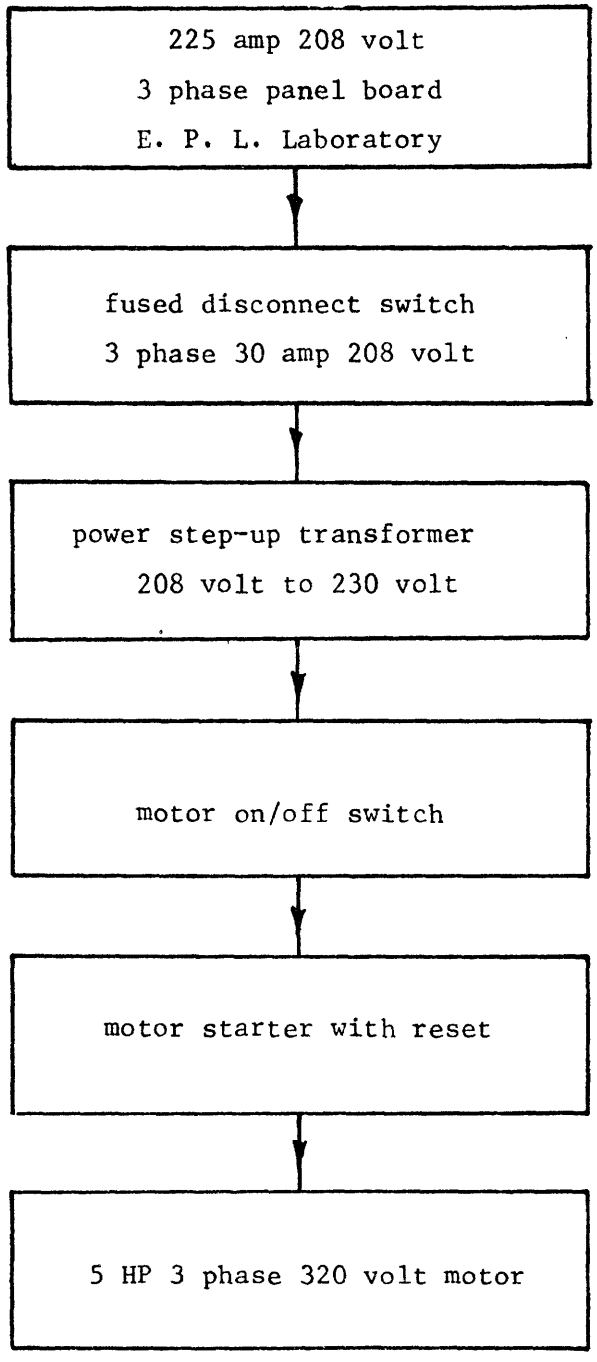

Electrical schematic for a 2 HP centrifugal pump rated at 50 GPM @ 50 ft. head

Figure 47

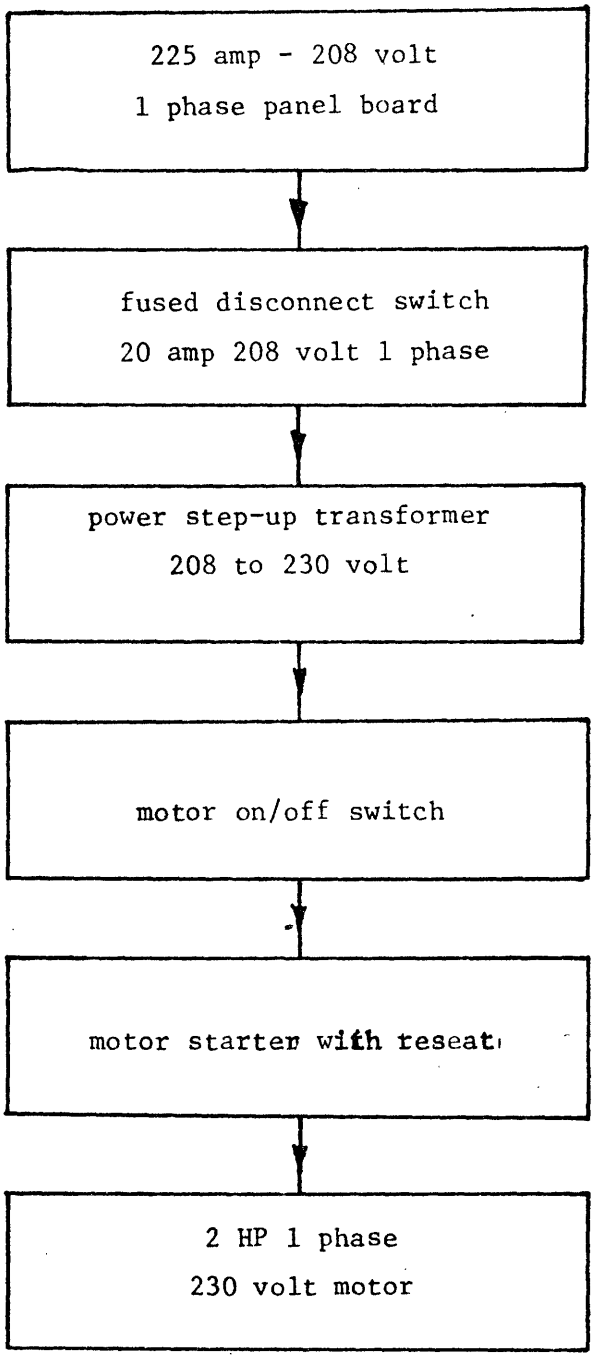

V. Conclusions and Recommendations

The flow visualization tests indicate the flow pattern of the water in the trough is largely determined by the rotating plates. Knowing the position of the water jet and its exit velocity, the flow path of the water entering the trough can be determined qualitatively.

The low viscosity silicone oil, with specific gravity less than one and negligible evaporation, can be used in the rotary heat exchanger to suppress water evaporation. With smooth plates of diameter 20 inches and angular velocity up to 30 r.p.m., no thorough mixing of the silicone oil with water was observed.

The heat transfer performance of the rotary heat exchanger will be tested with (1) smooth plates and (2) roughened plates to determine its feasibility.

The roughened surface is based on the existing correlation to predict the heat transfer coefficient and friction factor. However, the correlation is not based upon the same geometry and flow conditions as exhibited by the periodic heat exchanger. Future work will be concentrated on the effects of the flow angle of attack on the heat transfer coefficient and friction factor for the periodic heat exchanger. An experimental apparatus will be built to experimentally test different flow attack angles and different roughness dimensions. Another problem is to test the effect of the coating oil thickness on the square-ribs of the rough surface heat exchanger. This is essentially a question of how much the heat transfer coefficient and friction factor will be changed due to the coating oil creating fillets and rounds on the square-ribs of the periodic heat exchanger.

The periodic heat exchanger described in this report has been constructed for the purpose of testing actual performance characteristics of this new design approach. The full scale model of the periodic heat exchanger has been constructed, with the exception of the discs and air baffles for the test section, Calibration curves should be made for the contraction cone following the guide lines of section IV.2. Work on the design of the test discs, including disc stiffeners and turbulence promotors should continue until a satisfactory test section has been completed. Test data should then be compiled that will optimize total system performance. Various types of inlet sections which could be used in an actual field installation should be designed and tested. Plans of the optimized

system components should be drawn and submitted to interested companies for construction type bids to be used in evaluating the competitiveness of the optimized system with conventional systems.

REFERENCES

1. Robertson, M.W., Glicksman, L.R., and Rohsenow, W.M., "Improvement of the Environmental and Economic Characteristics of Cooling Towers', Part II: Periodic Cooling Towers", M.I.T., EPL Report No. 80047-82, June, 1973.

2. Noll, W., Chemistry and Technology of Silicones, Academic Press, New York, 1968.

3. Andeen, B.R., and Glicksman, L.R., "Dry Cooling Towers for Cooling Plants" Report No. 73047-1, M.I.T., February 1972.

4. Andeen, B.R., Glicksman, L.R., and Rohsenow, W.M., "Improvement of the Environmental and Economic Characteristics of Cooling Towers", Report No. 80047-82, M.I.T., June 1973.

5. Webb, R.L., Eckert, E.R., and Goldstein, R.J., "Heat Transfer and Friction in Tubes with Repeated-Rib Roughness," Int. J. Heat Mass Transfer, Vol. 14, pp. 601-617, 1971.

6. Webb, R.L. and Eckert, E.R., "Application of Rough Surfaces to Heat Exchanger Design" Int. J. Heat Mass Transfer, Vol. 15, pp. 1647-1648, 1972.

7. Veniamin, Levich, "Physicochemical Hydrodynamics", Prentice-Hall, Englewood Cliffs, N.Y. (1967).

8. Hansen, C.E., "The Design and Construction of a Low-Noise, Low-Turbulence Wind Tunnel", Report No. 79611-1.

9. Gorlin, S.M. and Slesinger, Wind Tunnels and Their Instrumentation, N.A.S.A., 1966.

10. Pope, A. and Harper, J.J., Low Speed Wind Tunnel Testing, John Wiley & Sons, New York, 1966.

11. Streeter, V.L., Fluid Mechanics, McGraw-Hill, New York, 1962.

12. Dryden, H.L. and Schubauer, G.B., "The Use of Damping Screens for the Reduction of Wind Tunnel Turbulence", J.A.S., April 1947.

13. Tsien, Hsue-Shen, "On the Design of the Contraction Cone for a Wind Tunnel" J.A.S. Vol. 10, p. 67, February 1943.

14. Mastrello, L., "Air Duct Facility for Investigation of Vibration Noise Induced by Turbulent Flow Past a Panel", U.T.I.A. Technical No. 20, April 1953.

15. Carrier Air Conditioning Co. Handbook of Air Conditioning Design, McGraw-Hill, New York, 1965.

16. Squire, H.B., "Jet Flow & its Efforts on Aircraft," Aircraft Engineering, Vol. XXII, p. 62-67, 1950.

APPENDIX A

For a power plant of 1000 MW, the heat transfer per plate of the rotary heat exchanger was estimated to be 4720 BTU/hr [1]. With a temperature drop of 5°F, the mass flowrate of water through per plate spacing is 4720/5 lbm/hr. In the full-scale rotary heat exchanger,

D = plate spacing = 1 inch

d = diameter of jet exit = 1/4 inch

R = radius of plate 2.5 ft.

ρ = density of water - 62 lbm/cu.ft.

the exit velocity of the water jet is 12.4 ft. per sec. With ω = angular velocity of the rotating plates = 10 r.p.m., the plate circumferential velocity = 2.62 ft/sec.

Since the inertia force dominates the flow pattern of the water, the important parameter in scaling is the ratio of the jet exit velocity to the plate circumferential velocity (with geometric similarity). In the 1/3 full scale model, the flow visualization tests were run with ω = 30 r.p.m., thus maintaining the same circumferential velocity as in the full-scale rotary heat exchanger. The jet exit velocity was also controlled at 12.4 ft/sec.

APPENDIX B

By comparing the water jet velocity and the plate velocity, we can estimate how far beyond the plate circumference the water jet can travel.

V_p = plate velocity = $R\omega$

R = radius in feet

ω = angular velocity of rotating plates = 10 r.p.m.

Therefore V_p = 1.048 R ft/sec.

The problem of the decay of a round jet into an infinite body of water was investigated thoroughly by many people, and its solution can be found in "Boundary Layer Theory" by Hermann Schlichting. However, based on experimental data, Squire [16] suggested for engineering purpose a much simpler formula:

$(V\ x)/(V_e\ d) = 6.5$ where

V = axial velocity of jet

V_e = exit velocity of jet = 12.4 ft/sec

d = diameter of jet exit = 1/4 inch

x = distance from jet exit

Therefore V = 20.2/x.

Plots of V_p vs r and V vs x are shown in figure A.1. It is seen that the jet velocity dominates only in the region a few inches beyond the plate circumference and close to the jet exit.

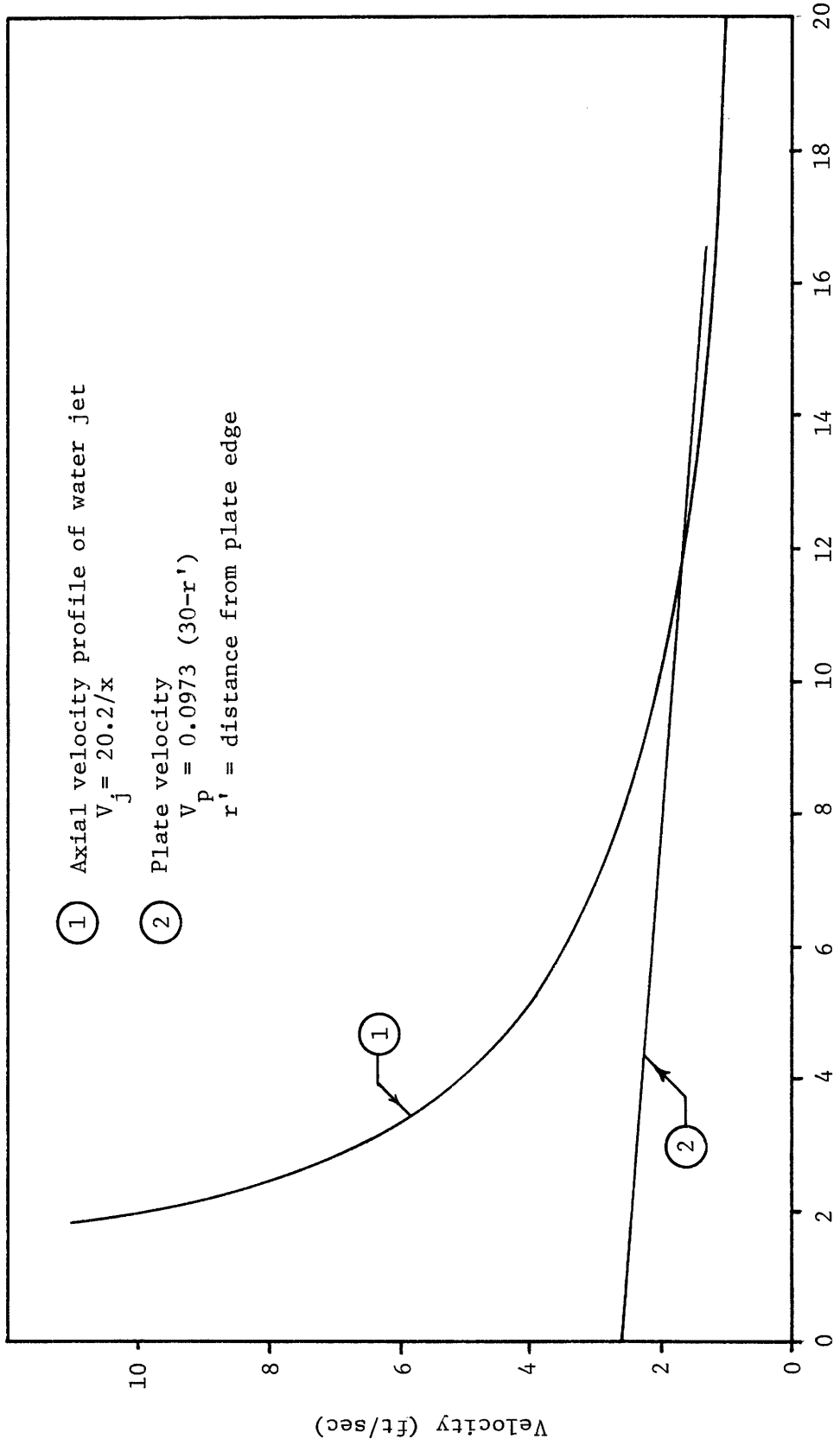

JET AND PLATE VELOCITY AS A FUNCTION OF DISTANCE

Figure A.1